INTEGRATION OF MICROVASCULAR, INTERSTITIAL, AND LYMPHATIC FUNCTION TO DETERMINE THE EFFECT OF THEIR INTERACTION ON INTERSTITIAL FLUID VOLUME

A Dissertation

by

RANJEET MANOHAR DONGAONKAR

Submitted to the Office of Graduate Studies of
Texas A&M University
in partial fulfillment of the requirements for the degree of

DOCTOR OF PHILOSOPHY

December 2008

Major Subject: Biomedical Sciences

INTEGRATION OF MICROVASCULAR, INTERSTITIAL, AND LYMPHATIC FUNCTION TO DETERMINE THE EFFECT OF THEIR INTERACTION ON INTERSTITIAL FLUID VOLUME

A Dissertation

by

RANJEET MANOHAR DONGAONKAR

Submitted to the Office of Graduate Studies of
Texas A&M University
in partial fulfillment of the requirements for the degree of

DOCTOR OF PHILOSOPHY

Approved by:

Chair of Committee,	Christopher M. Quick
Committee Members,	Glen A. Laine
	Randolph H. Stewart
	John C. Criscione
Head of Department,	Glen A. Laine

December 2008

Major Subject: Biomedical Sciences

ABSTRACT

Integration of Microvascular, Interstitial, and Lymphatic Function to Determine the Effect of Their Interaction on Interstitial Fluid Volume.

(December 2008)

Ranjeet Manohar Dongaonkar, B.E., Dr. Babasaheb Ambedkar Marathwada University;

M.S., Texas A&M University

Chair of Advisory Committee: Dr. Christopher M. Quick

Although the physics of interstitial fluid balance is relatively well understood, clinical options for the treatment of edema, the accumulation of fluid in the interstitium, are limited. Two related reasons for this failure can be identified. First, the processes involved in the transfer of fluid and proteins into the interstitium from the microvasculature, and their transfer out of the interstitium via the lymphatic system, are governed by complex equations that are not amenable to manipulation by physiologists. Second, the fundamental processes involved include complex anatomical structures that are not amenable to characterization by engineers. The dual tools of the batwing model and simplified mathematical modeling can be used to address the main objective: *to integrate microvascular, interstitial, and lymphatic function to determine the effect of their interaction on interstitial fluid volume.* In order to address this objective and the limitations of the current state of knowledge of the field, three specific aims were achieved. 1) Develop a simple, transparent, and general algebraic approach that predicts

interstitial fluid pressure, volume and protein concentration resulting from the interaction of microvascular, interstitial and lymphatic function. These algebraic solutions provide a novel characterization of interstitial fluid pressure as a balance point between the two processes that determine interstitial inflow and outflow. 2) Develop a simple, algebraic formulation of Edemagenic Gain (the change in interstitial fluid volume resulting from changes in effective microvascular driving pressure) in terms of microvascular, interstitial and lymphatic structural parameters. By separating the structural parameters from functional variables, this novel approach indicates how these critical parameters interact to determine the tendency to form edema. 3) To expand the list of known interactions of microvascular, interstitial, and lymphatic functions to include the direct interaction of venular and lymphatic function. Venomotion was found not only to extrinsically pump lymph but also to mechanically trigger intrinsic lymphatic contractions. These three advances together represent a new direction in the field of interstitial fluid balance, and could only be possible by taking an interdisciplinary approach integrating physiology and engineering.

DEDICATION

To my mom and dad

ACKNOWLEDGEMENTS

I would like to express my utmost gratitude to my PhD advisor, Dr. Christopher Quick, for his patience, guidance, and mentorship. He inspired and motivated me in more than one way at several times during my graduate career. He supported me during a crucial phase in my life when I decided to change majors from mechanical engineering to biomedical sciences and I will forever be grateful to him for that.

I would like to thank my committee, Dr. Glen Laine, Dr. Randolph Stewart, and Dr. John Criscione, for their support, guidance, and faith. Their feedback toward my research in the committee meetings was priceless.

I would also like to thank my lab mates for their feedback and constructive critiquing of my work.

My graduate school journey would have been incomplete without the support and humor of the innumerable friends I have had.

My parents and sister are my biggest inspiration and strength. Their boundless patience and belief in me encouraged me all through my graduate career.

TABLE OF CONTENTS

Page

1. INTRODUCTION

1.1 BACKGROUND

Interstitial inflow: interstitial fluid pressure and protein concentration determine flow of microvascular fluid and proteins into the interstitium. The fluid filtration rate across a microvascular membrane, originally described by the Starling Hypothesis (139), is a result of an imbalance between two competing forces—hydrostatic and colloid osmotic pressures (95, 120). A decrease in interstitial fluid pressure increases the hydrostatic pressure gradient, driving the fluid into the interstitium. A decrease in interstitial protein concentration, however, increases the colloid osmotic pressure gradient, maintaining fluid in the microvasculature. The two structural parameters that modulate the effects of these forces are the microvascular filtration coefficient (K_f), characterizing the permeability to water, and the reflection coefficient (σ), characterizing the relative permeability to proteins. On the other hand, the protein transfer rate across microvascular membrane is a result of convection due to fluid filtration and diffusion due to a protein concentration gradient. A decrease in interstitial fluid pressure increases the fluid filtration rate, driving proteins into the interstitium. A decrease in interstitial protein concentration increases the protein concentration gradient, also driving proteins into the interstitium. The two structural parameters that modulate these two processes are the reflection coefficient (σ) and the product of microvascular protein permeability and the microvascular surface area (PS) (147). In transfer of both fluid and proteins,

---

This dissertation follows the style of *American Journal of Physiology.*

interstitial fluid pressure and protein concentration thus play significant roles. Perhaps the complexity of interstitial fluid and protein dynamics has masked the fact that inflow and outflow can have a significant effect on interstitial fluid pressure (P_i) and protein concentration (C_i) (5, 65, 142). Typically, the values of P_i and C_i are assumed constant, i.e., unaffected by changes in interstitial inflow (40).

Interstitial outflow: interstitial fluid pressure determines flow of fluid and proteins out of the interstitium. The lymphatic system drains fluid and proteins from the interstitium. Characterizing the function of a single lymphatic vessel is complicated by the interplay of the axial pressure gradient, transmural pressure, and endothelial shear stress (7, 54, 55, 75, 106). Characterizing the function of an entire lymphatic system, however, is relatively simple, since the lymphatic system pressure-flow relationship can be linear over a large range of pressures (5, 22, 23). In a series of articles, Drake et al. successfully characterized the lymphatic pressure–flow relationship with two empirically-derived parameters—the effective lymphatic resistance (R_L) and the effective pump pressure (P_p) (39, 42, 44, 91, 93). As interstitial fluid pressure increases, the resulting increase in axial pressure gradients and transmural pressures act in concert to increase lymph flow (75). A recent study related the values of R_L and P_p to the mechanical properties of lymphatic vessels, including vessel contractility and contraction frequency (34). Although investigators have used Drake's formulation to predict the interaction of one part of a lymphatic system with another (143), this powerful description has not yet been used to address lymphatic-microvascular

interaction. In fact, a significant number of studies neglect the effect of lymphatic function on interstitial fluid balance (40).

Conservation of mass: edema is conventionally characterized as an imbalance of interstitial inflow and outflow. The process of interstitial fluid volume and protein regulation is typically characterized by invoking the principle of conservation of mass. The difference between interstitial inflow and outflow rates determines the rate of change in interstitial fluid volume and proteins. That is, when the inflow rate is greater than the outflow rate, the amounts of interstitial fluid and proteins increase. Conversely, when the outflow rate is greater than the inflow rate, the amounts of interstitial fluid and proteins decrease. The principle of conservation of mass is powerful, but limited. For instance, if only microvascular filtration is elevated experimentally, then gravimetric approaches can be used to ascribe changes in interstitial fluid volume to changes in microvascular permeability (40). However, measurement of interstitial fluid volume alone does not reveal whether microvascular filtration has increased or lymphatic function has decreased. In fact, once edema is established, inflow is equal to outflow, and no information is available to determine whether microvascular or lymphatic function has been compromised. Furthermore, the amount of microvascular filtration and lymph flow in steady-state is not directly related to interstitial fluid volume–edema can be associated with both high and low flows (34). Finally, because both conservation of mass and balance of forces are necessary to characterize mechanical systems from fundamental principles (51), characterization of edema as a mismatch of inflow and

outflow is theoretically incomplete. Taken together, conservation of mass is necessary, but not sufficient, to characterize interstitial fluid balance.

Interstitial storage: interstitial compliance is conventionally believed to determine interstitial fluid pressure. The interstitium's capacity to store fluid is a fundamental mechanical property characterized by the "interstitial compliance", the slope of the interstitial fluid volume-pressure relationship (63, 131). Interstitial compliance is believed to play a fundamental role in interstitial fluid balance—it determines how much interstitial fluid pressure rises with an increase in interstitial fluid volume. Three related concepts follow. First, the extraordinarily high interstitial compliance reported for the lung may prevent complications arising from edema (63, 140). In this case, interstitial fluid volume can significantly increase without a concomitant increase in interstitial fluid pressure, thus preventing alveolar flooding (63, 140). Second, decreasing the effective interstitial compliance with compressive sleeves may reduce peripheral edema by raising interstitial fluid pressure (17, 23). In this case, reduction of interstitial fluid volume follows from diminished microvascular filtration and enhanced lymphatic drainage. Third, increasing interstitial compliance with pharmacological agents or focal injury may induce edema by decreasing interstitial fluid pressure (132). In this case, the lower interstitial fluid pressure draws fluid into the interstitium from the microvascular space. Inherent in all three concepts, a change in interstitial compliance is believed to alter the equilibrium interstitial fluid pressure.

Venules and lymphatic microvessels modulate interstitial fluid volume. It is believed that lymphatic microvessels developmentally derive from venules (118, 138),

and they not only share similar structure, but also are often located within microns of each other (150). Venules function to moderate microvascular fluid pressure, and thus the driving pressure for transmicrovascular flux (27, 28, 59, 78). Lymphatic microvessels, however, play a central role in regulating not only interstitial fluid volume but also the turnover of interstitial proteins (69, 144). Lymph, interstitial fluid that has entered the initial lymphatics, is transported by intrinsic as well as extrinsic mechanisms via a system of converging conducting lymphatic vessels to the lymph nodes and then to the great veins of the neck. Since lymph flow is inhibited by increases in central venous pressure (i.e., the lymphatic outlet pressure), venous and lymphatic functions are coupled at their outlets as well as at their inlets (36, 91). Although venules typically can be found within microns of parallel lymphatic microvessels (150) and both play a critical role in regulating the local environment of the interstitium, venular and lymphatic microvascular functions are conventionally described as *indirectly* coupled.

Lymph is actively propelled by extrinsic mechanical compression. Lymphangions, the segments of lymphatic vessels between two unidirectional valves, provide the structure that allows lymph to be actively propelled from the low-pressure interstitial space to the higher-pressure veins (144, 167). Although it is recognized that cyclical contraction of muscular lymphatic vessels can propel lymph, external compression is the only means of propulsion in the intestinal wall, skeletal muscle, heart, and lung, where lymphatic microvessels are devoid of lymphatic smooth muscle (136). In these organs, lymph formation and propulsion depends solely on periodic extrinsic expansion and compression of lymphangions by surrounding tissues (96, 105). Schmid-

Schönbein et al., suggested that in addition to contractions of the surrounding muscle, arteriolar vasomotion may also extrinsically propel lymph from initial lymphatic vessels in skeletal muscle (135, 137). In organs such as skin, which is not surrounded by periodically contracting tissues, it is believed that intrinsic pumping is necessary to propel lymph.

Mechanical stimuli modulate intrinsic pumping of the lymphatic vessel. Contraction of lymphatic muscle, leading to the intrinsic pumping of lymph, is modulated by mechanical factors. First, tension in the filaments tethering lymphangions to the interstitium can passively enhance filling from upstream lymphangions or from the surrounding interstitium (20). Second, stretch of lymphatic muscle is known to enhance pacemaker activity and thus increase the frequency and strength of lymphangion contraction (7, 75, 106). This mechanism has been proposed to increase lymphangion pumping with increased tissue hydration (7). Furthermore, a rapid stretch is known to trigger an intrinsic contraction of vascular smooth muscle (116), which is one mechanism that can cause a lymphangion to contract after being filled by an upstream lymphangion. Each mechanism allows a lymphatic vessel to respond to the mechanical forces in its immediate environment. The sensitivity of lymphatic function to common anesthetics, trauma resulting from exteriorizing lymphatic beds, and even contrast agents used for visualization (2, 26, 77, 107), have limited the investigation of the role of mechanical forces on lymphangion function in vivo.

There are multiple explanations for histamine-induced pulmonary edema. The difficulty in ascribing changes in interstitial fluid volume to a particular volume-

regulating phenomenon is put in bold relief by the example of histamine. Infusion of histamine induces edema within minutes (88, 111, 124). Some reports ascribe this effect to increased transmicrovascular fluid flux due to increased permeability or vascular surface area (11, 88, 108, 115, 124). Lymph flow is reported to increase with histamine infusion (3, 11, 19, 33, 46, 73, 108, 115, 133) either by increased contraction rate (47) or by increased strength of contraction (76, 133, 146). However, inhibition of lymph flow with intravenous infusion of histamine at high concentrations (> 5μM) (47, 127) has also been reported, and thus the lymphatic system may play a role. Yet another mechanism for edema formation has been postulated that does not require changes in permeability or lymphatic function. Histamine has been reported to increase interstitial compliance (3, 130). That is, given the same interstitial fluid pressure, the interstitium can accommodate a much larger volume of fluid. The resulting change in compliance alone is capable of producing edema in skin and skeletal muscle (130, 160). This example illustrates a common difficulty in edema research—multiple mechanisms can lead to edema, and current analytical tools are not able to determine their relative contributions.

2. DISSERTATION OBJECTIVES

Analysis of the literature presented in Section 1 provides the insight that guides the focus of this Dissertation. First, fluid volume and pressure are typically characterized as a function of either microvascular (11, 88, 108, 115, 124), lymphatic (47, 127), or interstitial (3, 130, 160) function. Although microvascular function has been characterized algebraically, the lack of a simple description of lymphatic function has hindered the integration of these three functions. One such analytical description by Drake et al. (38) has yet to be used in such formulations. Although it is evident that interstitial fluid pressure and protein concentration play critical role, the relative contributions of lymphatic function and microvascular function to interstitial fluid volume and pressure is not well understood. This has led to a number of complications, including ascribing changes in interstitial fluid volume solely to either changes in microvascular function (characterized by the filtration coefficient) (11, 88, 108, 115, 124), changes in interstitial function (characterized by interstitial tissue compliance) (3, 130, 160) or lymphatic function (characterized by lymphatic pump function) (47, 127). The particular function that an investigator identifies as a cause for an observed change in interstitial fluid volume typically depends on the starting set of assumptions or professional focus of the investigator. It is necessary to integrate these three functions to explore how the whole of interstitial fluid regulation becomes more than the sum of its constituent parts.

Second, the sensitivity of tissues to an edemagenic challenge is as important as the degree of edema. Edema can be both a cause and an effect (14, 24, 125) of major morbidity such as cardiac, renal and pulmonary failure. The techniques used to determine the degree of edema, however, have limited prognostic potential. For instance, different inflammatory agents such as histamine and endotoxin can result in similar degrees of edema, although edema secondary to endotoxin is more likely to worsen with increased microvascular pressure (1, 92). Despite a focus on anti-edema mechanisms, investigators have neglected to address this sensitivity of edema formation to edemagenic challenges. Though the concept of a "gain" has been used to characterize whole-body fluid balance (64), it has yet to be applied to interstitial fluid balance. The potential exists to bridge the gap between basic physiology and clinical practice, since the complexity of interstitial fluid balance results from three relatively simple phenomena—interstitial inflow, interstitial inflow, and interstitial fluid storage. However, it is first necessary to develop a simple algebraic formula that explicitly illustrates how the critical structural parameters interact to regulate interstitial volume.

Third, although a direct interaction has been experimentally demonstrated between microvascular and interstitial function (48, 56, 104, 141) or interstitial and lymphatic function (21, 145, 168), it has been assumed that microvascular and lymphatic function are indirectly coupled (36, 91). The role of vasomotion, in particular, has been neglected. Arterioles as well as venules are observed to exhibit vasomotion, active spontaneous contractions. Venomotion, i.e., venular vasomotion, involves a large change in diameter. As a result, tissue surrounding venules adjacent to lymphatic vessels

experiences compression and expansion during venular dilation and contraction. Since lymphatic microvessels can be found in close proximity of venules exhibiting venomotion, venules may directly affect the mechanical environment of lymphatic microvessels through venomotion. Although the role of arteriolar vasomotion in extrinsic propulsion of lymph in skeletal muscle has been characterized, the sensitivity of venomotion as well as lymphatic function to common anesthetics and trauma may have limited the characterization of venular-lymphatic interaction. There is a critical need for an animal model that does not require anesthetics or surgical exteriorization of the microvasculature to study the possible direct interaction of venular and lymphatic function.

Two major reasons can be identified why these three problems have not yet been addressed in the literature. First, few investigators have applied simplified mathematical modeling to integrate interstitial fluid volume and protein regulation. Second, there is a critical lack of animal models appropriate to test hypotheses.

The individual processes involved in interstitial fluid volume and protein regulation are simple. However, the integration of these simple processes has yielded complex results that have obscured elucidation of their interaction. The presence of the negative feedback and the derivative introduced in the equation characterizing interstitial fluid balance, in particular, have limited to tools available for conventional mathematical modeling. To deal with these complications, most of investigators have relied on complex mathematical models that require numerical solutions. However, numerical approaches have a number of inherent limitations; the most critical of which is the lack

of general solution. Numerical approaches result in specific solutions valid only for specific known values of parameters used in the simulation. Second, separate plots are needed to determine the effect of any one of a long list of parameters and variables: microvascular pressure, plasma colloid osmotic pressure, water permeability, interstitial compliance, effective lymphatic resistance, venous pressure. Furthermore, the inability to view the effect of more than one parameter on interstitial fluid volume and pressure makes it impossible to grasp the complex interaction between interstitial inflow and outflow. The small error incurred when making simplifying assumptions to arrive at an algebraic solution (explicitly relating system function to its structure) can be worth the insight gained with a simple formula.

Venomotion was first observed in the bat wing over a hundred and fifty years ago (81), in part, because the thin translucent wing made it possible to study the intact microvasculature noninvasively without the confounding effects of surgery, anesthesia, or contrast agents. Bat wing preparations have since been used to make fundamental advancements in the understanding of vascular innervation (155), the myogenic response (16, 31), shear-induced dilation (29, 152), arteriolar and venular vasomotion (15, 148, 154), and capillary recruitment (153). Most vascular responses have been shown to be similar to more common animal models such as the hamster cheek pouch, rat mesentery, and cremaster muscle, although bat wing responses are often more robust (29, 31). Since venomotion is diminished by common anesthetics (26), the unanesthetized bat wing model is particularly advantageous for studying venomotion.

The dual tools of the batwing model and simplified mathematical modeling can be used to address the main objective: *to integrate microvascular, interstitial, and lymphatic function to determine the effect of their interaction on interstitial fluid volume.* In order to address this objective and the limitations of the current state of knowledge of the field, three specific aims must be achieved. 1) To develop a simple, transparent, and general algebraic approach that predicts interstitial fluid pressure, volume and protein concentration resulting from the interaction of microvascular, interstitial and lymphatic function. These algebraic solutions will provide a novel characterization of interstitial fluid pressure as a balance point between the two processes that determine interstitial inflow and outflow. 2) Develop a simple, algebraic formulation of Edemagenic Gain (the change in interstitial fluid volume resulting from changes in effective microvascular driving pressure) in terms of microvascular, interstitial and lymphatic structural parameters. By separating the structural parameters from functional variables, this novel approach will indicate how these critical parameters interact to determine the tendency to form edema. 3) To expand the list of known interactions of microvascular, interstitial, and lymphatic functions to include the direct interaction of venular and lymphatic function. It is hypothesized that venomotion not only acts to extrinsically pump lymph but also to mechanically trigger intrinsic lymphatic contractions. The following sections will address each of these specific aims.

Section 3: By integrating lymphatic function into the set of standard fluid balance equations, interstitial fluid volume and protein regulation will be formulated algebraically in terms of parameters characterizing microvascular, interstitial, and

lymphatic function. General algebraic solutions for steady-state interstitial fluid pressure and protein concentration will be derived using this formulation. This approach will result in the novel finding that interstitial compliance does not affect steady-state interstitial pressure.

Section 4: A simple solution to the standard fluid balance equations will be developed by making critical simplifying assumptions. Reformulation of the classical equations governing fluid balance as transfer functions will yield a novel index: the Edemagenic Gain. This approach will result in the novel finding that there are two types of edema: multivariate edema and compliance-dominated edema.

Section 5: The Pallid bat wing model will be used to simultaneously record diameters of venules and adjacent lymphatic microvessels and evaluate the temporal relation between their contractions. Two possible mechanisms for interaction will be explored: direct compression of lymphatic vessels by the expanding venule during venomotion, and the potential for movement of an adjacent venule to mechanically trigger lymphatic contraction. This approach will result in the novel finding that with venular-lymphatic coordination; extrinsic and intrinsic lymph pumping mechanisms may not only coexist, but also are coordinated.

Section 6: Results from Sections 3-5 will be discussed, and implications to the new understanding of interstitial fluid balance will be identified.

3. INTEGRATING MICROVASCULAR, INTERSTITIAL, AND LYMPHATIC FUNCTION WITH A BALANCE POINT CHARACTERIZATION OF INTERSTITIAL FLUID VOLUME AND PROTEIN REGULATION

3.1 METHODS

Interstitial inflow of fluid. The Starling-Landis Equation (*Eq. 3.1*) characterizes the fluid filtration rate (J_V) across microvascular membrane into the interstitium (95, 120). The transmicrovascular fluid flow rate is determined by the microvascular filtration coefficient (K_f) in response to effective microvascular driving pressure resulting from hydrostatic and colloid osmotic pressure gradients. The difference between microvascular (P_c) and interstitial (P_i) hydrostatic pressures tends to force fluid into the interstitium. The value of K_f depends on microvascular surface area and permeability to water. The difference between microvascular (Π_c) and interstitial (Π_i) colloid osmotic pressures tends to draw fluid in the opposite direction, from the interstitium into the microvessels. The reflection coefficient (σ) characterizes the relative permeability of the microvasculature to plasma proteins (having a value between 0 and 1), and thus modulates the contribution of colloid osmotic pressure to effective microvascular driving pressure.

$$J_V = K_f \left[(P_c - P_i) - \sigma(\Pi_c - \Pi_i) \right] \qquad (3.1)$$

To be consistent with rest of the analysis, Starling-Landis Equation is formulated in terms of plasma (C_c) and interstitial protein (C_i) concentration given by *Eq. 3.2* and will be used henceforth.

$$J_V = K_f \left[(P_c - P_i) - \alpha\sigma(C_c - C_i) \right] \quad (3.2)$$

When concentration is in *moles*/*kg*, α can be estimated by $R \cdot T$, where R is the ideal gas constant and T is absolute temperature (151). When concentration is in *mg*/*ml*, an experimentally derived value for α is used (70, 71). Consistent with previous work (34), P_c, P_i, C_c, and C_i are considered variables, and K_f and σ are considered structural parameters.

Interstitial inflow of proteins. The microvascular protein extravasation rate (J_{sV}) (i.e., the interstitial inflow of proteins) is characterized using the linear Taylor-Granger Equation (*Eq. 3.3*) (6, 147). In this formulation, protein flux across microvascular membrane is determined by convective as well as diffusive processes. The microvascular fluid filtration rate (J_V) drives the convective transfer of proteins, and is modified by C_c and σ. The protein concentration gradient across microvascular membrane (C_c-C_i) drives protein diffusion, and is modified by the microvascular protein permeability-surface area product (*PS*).

$$J_{sV} = J_V (1 - \sigma) C_c + (C_c - C_i) PS \quad (3.3)$$

Although, this formulation is based on an approximation proposed by Kedem et al. (84) that treats diffusion and convection as independent processes, comparison with other formulations suggested that the Taylor-Granger formulation better approximates the well-accepted nonlinear Patlak-Hoffman (123) formulation (*Eq. C2*) (see *Appendix C*).

Interstitial outflow of fluid. The Drake-Laine Equation (*Eq. 3.4*) characterizes lymphatic function by relating lymph flow rate (J_L) to an effective lymphatic driving pressure (38). Since lymphatic outlet pressure (P_{out}) is typically greater than interstitial

fluid pressure (P_i), the difference in P_i and P_{out} tends to retard lymph flow. The value of (P_i+P_p) represents the lymphatic driving pressure and is composed of interstitial hydrostatic pressure and lymphatic pumping pressure (P_p). The effective lymphatic resistance (R_L) is the slope of the relationship between effective lymphatic driving pressure (P_i+P_p-P_{out}) and the resulting lymph flow.

$$J_L = \frac{(P_i + P_p - P_{out})}{R_L} \tag{3.4}$$

In this formulation P_p and R_L are empirically-derived parameters used to describe the lymphatic pressure-flow relationship (38), and are not necessarily equivalent to pressure developed by lymphatic vessel contraction or resistance to lymph flow. Recently, P_p and R_L were related to lymphatic contractility and contraction frequency (34).

Interstitial outflow of proteins. Although lymph protein concentration can deviate from C_i, for simplicity, it is assumed in this work that they are equal. That is, with no protein concentration gradient across lymphatic membrane, the interstitial outflow rate of proteins is determined by a convective process only. Using the Drake-Laine Equation (*Eq. 3.4*) to characterize the lymphatic fluid drainage rate (J_L) driving convection, the rate of lymphatic drainage of interstitial proteins (J_{sL}) takes on a simple form.

$$J_{sL} = C_i J_L = C_i \frac{(P_i + P_p - P_{out})}{R_L} \tag{3.5}$$

Characterizing steady-state conditions. A steady-state condition is reached when the rates of interstitial inflow and outflow of both fluid and proteins are balanced. At steady-state, interstitial fluid volume and protein assume constant values (*Eq. 3.6*).

$$J_V = J_L \tag{3.6a}$$

$$J_{sV} = J_{sL} \tag{3.6b}$$

Characterizing interstitial storage. The interstitium's capacity to store fluid is a fundamental mechanical property characterized by the "interstitial compliance", the slope of the interstitial fluid volume-pressure relationship (63, 131). The relationship between interstitial fluid pressure and volume can be highly nonlinear (63, 131). Typically, under normal conditions, interstitial fluid pressure is sensitive to changes in interstitial fluid volume (i.e., C is small). With overhydration, the compliance can become much larger, and the sensitivity of interstitial fluid pressure to interstitial fluid volume is lost (63). To capture this behavior, the interstitial fluid pressure-volume relationship has been approximated to be "piecewise linear," a commonly used technique to deal with the effect of hydration on interstitial compliance (12, 22, 70). Interstitial storage of proteins is characterized by the ratio of total interstitial protein (Q) and interstitial fluid volume (IFV).

$$P_i = \frac{IFV - V_0}{C} \tag{3.7a}$$

$$C_i = \frac{Q}{IFV} \tag{3.7b}$$

In this case, V_0 is the intercept of the interstitial fluid volume-pressure relationship, C is the interstitial compliance.

Control theory approach. The individual subsystems that govern interstitial fluid volume and protein are relatively simple (*Eqs. 3.2-3.7*). However, their interaction can be complex, given that there is inherent feedback in the system. To simplify, the

regulation of interstitial fluid volume and protein are analyzed using the transfer function concept of classical control theory, commonly used to characterize systems with feedback (49). For analysis purposes, the sub-systems are assumed to be linear and time-invariant, meaning that they are characterized by structural parameters such as K_f, σ, R_L, and P_p, which are assumed to be constant over the period of interest. Variables such as P_c, P_i, C_c, Ci, and V are treated as either inputs or outputs to each subsystem. Block diagrams are then constructed to represent the transfer functions created from *Eqs. 3.2-3.7.*

3.2 RESULTS

Graphical representation of steady-state. The steady-state values of P_i and C_i can be represented graphically using a standard balance-point approach (62, 67). For illustration purposes, Fig. A-1A represents the interstitial fluid flow balance point. To construct it, first the relationship of P_i and J_V (*Eq. 3.2*) is plotted. Assuming that interstitial protein concentration is in equilibrium, this relationship is linear, with a slope of $-K_f$ and an intercept of $P_c-\alpha\sigma(C_c-C_i)$. Then the relationship of P_i and J_L (*Eq. 3.4*) is plotted. This relationship is also linear, and has a slope of R_L and intercept of $P_{out}-P_p$. Because $J_V=J_L$ at steady-state, these lines are placed on the same graph. The equilibrium between J_v and J_L is represented by the intersection, which yields the value of P_i in equilibrium. This equilibrium point is the interstitial fluid flow balance point. A similar process is used to graphically illustrate the interstitial protein flow balance point in Fig. A-1B, constructed from *Eqs. 3.3* and *3.5*.

Algebraic solutions characterizing equilibriums. As steady-state is reached, interstitial inflow rates are balanced with outflow rates, leading to constant interstitial fluid volume and protein content. To algebraically represent the interstitial fluid and protein balance points, *Eqs. 3.2-3.6* are solved simultaneously, assuming steady-state conditions represented by *Eq. 3.5* (*Eq. 3.8*).

$$P_i = \frac{K_f R_L}{(1+K_f R_L)}\left[P_c - \alpha\sigma(C_c - C_i)\right] + \frac{1}{(1+K_f R_L)}(P_{out} - P_p) \qquad (3.8a)$$

$$C_i = \frac{1}{\dfrac{P_i + P_p - P_{out}}{R_L} - \left[\alpha\sigma(1-\sigma)K_f C_c - PS\right]}\left[(1-\sigma)K_f(P_c - P_i - \alpha\sigma C_c) + PS\right]C_c \qquad (3.8b)$$

Notably, interstitial compliance (C), does not appear in these equations, indicating a non-intuitive result that interstitial compliance has no affect on interstitial fluid pressure (*Eq. 3.8a*). Substituting *Eqs. 3.8a* and *3.8b* into *Eqs. 3.4* and *3.5* yield equilibrium lymphatic outflow of fluid and protein.

$$J_L = \frac{K_f}{1+K_f R_L}\left[P_c - \alpha\sigma(C_c - C_i) + (P_p - P_{out})\right] \qquad (3.9a)$$

$$J_{sL} = \frac{(P_i + P_p - P_{out})\left[(1-\sigma)K_f(P_c - P_i - \alpha\sigma C_c) + PS\right]C_c}{P_i + P_p - P_{out} - \left[\alpha\sigma(1-\sigma)K_f C_c - PS\right]R_L} \qquad (3.9b)$$

Block-diagram representation of interstitial fluid volume and protein regulation. Figure A-2A illustrates the block-diagram representations of interstitial fluid volume regulation under steady-state conditions. Parts I and II represent microvascular driving pressure and lymphatic effective pumping pressure. A combination of $K_f R_L$ arises in simple transfer functions that modulate these driving pressures. P_i arises as a sum of the

two modified pressures I and II (corresponding to the left and right terms in *Eq. 3.8a*). Notably, *IFV* is revealed to be an output of a transfer function consisting of a parameter C characterizing the interstitial compliance, and results from the input P_i. The value of P_i itself is not affected by the value of C. Similarly, Fig. A-2B illustrates the block-diagram representation of interstitial protein regulation under steady-state conditions.

Estimation of P_i and C_i at steady-state. The algebraic formulas represented by *Eq. 3.8* were used to predict steady-state values of P_i and C_i in different organs. The resulting estimates of P_i and C_i were then compared with previously reported values of P_i and C_i derived experimentally (45, 74, 80, 94, 97, 160). Values of parameters (K_f, σ, R_L, P_p) were collected from various publications that used similar experimental models and conditions. Table B-1A illustrates the comparison between interstitial fluid pressure and protein concentration estimates with experimental measurements. The effect of a change in parameters K_f and σ was evaluated in the case of dog lung. Minimum and maximum values of these parameters reported in the literature were used to determine the range of resulting values of P_i and C_i (Table B-1B and B-1C). As K_f increased from the minimum to maximum reported values (0.07 to 0.11), P_i increased from -2.2 to -1.3 *mmHg* and C_i decreased from 31 to 30.7 *mg*/*ml* (Table B-1B). Similarly, an increase in σ from the minimum to maximum reported values (0.48 to 0.89) resulted in a decrease in P_i from -0.2 to -6.7 *mmHg* and a decrease in C_i from 36.6 to 22.9 *mg*/*ml* (Table B-1C).

4. EDEMAGENIC GAIN AND INTERSTITIAL FLUID VOLUME REGULATION*

4.1 METHODS: THEORY

The Starling-Landis Equation (*Eq. 3.1*) used to characterize microvascular fluid filtration and the Drake-Laine Model (*Eq. 3.4*) used to characterize lymphatic function are explained in previous section. In brief, the Starling-Landis equation relates microvascular fluid filtration rate (J_V) to effective microvascular driving pressure determined by microvascular (P_c) and interstitial (P_i) hydrostatic pressures and microvascular (Π_c) and interstitial (Π_i) colloid osmotic pressures. The reflection coefficient (σ) and microvascular filtration coefficient (K_f) modulate this relationship. The Drake-Laine Model (*Eq. 3.4*) relates lymph flow rate (J_L) to an effective lymphatic driving pressure (38) determined by interstitial hydrostatic pressure (P_i), lymphatic pumping pressure (P_p), and lymphatic outlet pressure (P_{out}). The effective lymphatic resistance (R_L) is the slope of the relationship between effective lymphatic driving pressure and the resulting lymph flow.

The nonlinear relationship of interstitial hydrostatic pressure and interstitial fluid volume is assumed to be simple piecewise linear relationship (*Eq. 4.1*). The slope of this relationship is the reciprocal of interstitial compliance (C),

---

* Reprinted with permission from "Edemagenic gain and interstitial fluid volume regulation" by R. M. Dongaonkar, C. M. Quick, R. H. Stewart, R. E. Drake, C. S. Cox, Jr., and G. A. Laine, 2008. *Am J Physiol Regul Integr Comp Physiol* 294: R651-R659, Copyright [2008] by The American Physiological Society.

$$P_i = P_o + \frac{1}{C} \cdot V \qquad (4.1)$$

where P_o is an empirical constant.

Interstitial fluid inflow rate (*Eq. 3.1*) and interstitial fluid outflow rate (*Eq. 3.4*) are both functions of interstitial fluid pressure, and thus, interstitial fluid volume (*Eq. 4.1*). Assuming conservation of mass, the rate of change of interstitial fluid volume (i.e., *dV*/*dt*) is equal to the difference in rates of interstitial inflow and outflow of fluid.

$$\frac{dV}{dt} = J_V - J_L \qquad (4.2)$$

With known values of parameters (P_p, C, R_L, K_f) and inlet and outlet pressures (P_c-$\sigma \cdot \Pi_c$ and P_{out}), *Eqs. 3.1, 3.4, 4.1, and 4.2* can be solved simultaneously for four unknown variables (J_V, J_L, P_i, and V) (see *Appendix D*). In the present approach, variations in interstitial colloid osmotic pressure (Π_i) are neglected. Previously published reports were reviewed to characterize the possible range of parameter values and summarized in Table B-2.

4.2 METHODS: EXPERIMENT

The experimental preparation has been described previously (53). Experiments were conducted in accordance with protocols approved by the University of Texas Medical School Animal Welfare Committee. Briefly, sheep (n = 20) were anesthetized with halothane. Using sterile technique, polyethylene catheters were placed into the pulmonary artery and left atrium through a left thoracotomy. A 30cc Foley balloon catheter was introduced into the left atrium, and fluid filled catheters into the right

atrium via either the azygous vein or the left femoral vein. The chest was closed, and the sheep were allowed to recover for approximately one week before the acute experiments. Postoperative antibiotics and analgesics were administered by veterinarians as clinically indicated.

This preparation allowed the measurement of pulmonary arterial (PAP) and left atrial pressures (LAP). A pressure control system was used to regulate the size of the left atrial balloon and control LAP in a subgroup of sheep (n = 5) (53). Pulmonary microvascular pressure (P_c) was estimated as the average of PAP and LAP (53). Solid-state pressure transducers, amplifiers and a chart recorder were used to record all pressures. The olecranon was chosen as the zero pressure reference level because it is near the level of the left atrium and was easily identified (53). Plasma colloid osmotic pressure (Π_c) was measured with a membrane osmometer. Sheep were euthanized after a 3 h period and the extravascular fluid weight/blood free dry weight ratio (EVF) was determined utilizing a modification of the method of Pierce (53).

Control experiments. The control relationship between EVF and P_c-Π_c in the lungs of 9 anesthetized sheep was previously determined (53). In order to confirm the consistency of the experiments, EVF in 2 additional control sheep was determined. In the first experiment, EVF was 3.9 after a 3 h period with no elevation in microvascular pressure (P_c-Π_c = -12.5) and in the second experiment EVF was 4.2 with P_c-Π_c = 5 mmHg. These EVFs were consistent with the EVF of 4.0±0.2 obtained in sheep without P_c elevation, and the EVF of 4.3±0.1 with P_c-Π_c = 5 mmHg. Therefore, the new data

was combined with the previously determined data to establish the relationship between control EVF and P_c-Π_c.

Histamine experiments. 4 μg/kg/min of histamine phosphate was infused into a total of nine sheep for a three hour period. In 7 sheep, histamine was infused into the systemic venous circulation, while in 2 other sheep it was infused into the pulmonary venous circulation. In five of these experiments, the pressure control system was used to control LAP so that P_c was either 0 or 5 mmHg higher than Π_c for the 3 h period. In four experiments, LAP was not elevated. Two protocols for histamine infusion were used to evaluate whether different histamine infusion locations affect EVF with or without LAP elevation.

4.3 METHODS: ANALYSIS OF PREVIOUSLY REPORTED DATA

Compliance estimation. To compare results of histamine infusion to increased systemic venous pressure, data previously reported by Laine et al. (90) was analyzed. Briefly, the effect of systemic venous pressure elevation on lung edema formation was determined by elevating superior vena caval pressure (SVCP) of anesthetized sheep (n = 8) by inflating a balloon occluder placed above the level of the azygos vein. Left atrial pressure was then controlled by partially inflating a balloon occluder inserted into the left atrium with and without elevating SVP to 10 mmHg for three hours. The amount of fluid present in the lung was determined from wet-to-dry weight ratios, similar to the current study.

Endotoxin infusion. Similarly, to compare results of histamine infusion to endotoxin infusion, data previously reported by Gabel et al. (53) was analyzed. Briefly, the effect of endotoxin infusion (1μg/kg) on lung edema formation was determined in anesthetized sheep (n = 6). LAP was varied by inflating a balloon occluder placed in left atrium. The amount of fluid present in the lung was determined from the wet-to-dry weight ratios, as in the current study. The resulting Edemagenic Gain for the endotoxin infusion group was compared to histamine and SVCP elevation groups.

4.4 RESULTS

Edemagenic Gain. Simultaneously solving *Eqs. 3.1, 3.4, 4.1, and 4.2* and rearranging (See details in *Appendix D*) results in a ratio of ΔV to $\Delta(P_c\text{-}\sigma\cdot\Pi_c)$. This new equation is termed "Edemagenic Gain" (*EG*).

$$\text{Edemagenic Gain} = \frac{\Delta V}{\Delta\left(P_c - \sigma\cdot\Pi_c\right)} = \frac{C\cdot R_L\cdot K_f}{1+R_L\cdot K_f} \qquad (4.3)$$

Edemagenic Gain can be expressed in the form of a classical feedback system relating the tendency to store excess interstitial volume to the parameters C, R_L and K_f. Edemagenic Gain is represented in the form of a "transfer function" relating an input variable, $\Delta(P_c\text{-}\sigma\cdot\Pi_c)$, to an output variable, ΔV (Fig. A-6A). The possible ranges of parameters derived from the literature are listed in Table B-2.

Compliance-Dominated and Multivariate gains. *Equation 4.3* degenerates into an even simpler form when the combination of $R_L\cdot K_f$ is either much greater or less than 1.

$$EG \approx \begin{cases} C, & R_L \cdot K_f >> 1 \quad \text{(Compliance – Dominated Gain)} \\ \dfrac{C \cdot R_L \cdot K_f}{1 + R_L \cdot K_f}, & R_L \cdot K_f << 1 \quad \text{(Multivariate Gain)} \end{cases} \tag{4.4}$$

When $R_L \cdot K_f$ is much larger than 1, Edemagenic Gain is "Compliance-Dominated", and when $R_L \cdot K_f$ is much less than 1, Edemagenic Gain is "Multivariate". Although K_f is smaller than 1, R_L can have fairly large values (see Table B-2). Therefore, the value of $R_L \cdot K_f$ is larger than 1 when R_L is elevated, even if K_f varies markedly. These results are summarized in Fig. A-6B.

Effect of histamine. Figure A-7 illustrates the change in EVF plotted as a function of P_c-Π_c for each experiment. The histamine EVFs were significantly higher than the control EVFs at baseline P_c-Π_c and for P_c-Π_c = 5 mmHg. The location of histamine infusion had no effect on EVF. In the two experiments with histamine infusion into the pulmonary venous circulation, EVFs were 4.7 without LAP elevation and 4.9 with LAP elevation. These EVFs were consistent with EVFs from the experiments with histamine infusion into the systemic venous circulation (with EVFs 4.5±0.2 without LAP elevation and 5.1±0.3 with LAP elevation). The estimate of Edemagenic Gain for the control group is 0.018 ml/g·mmHg, and 0.034 ml/g·mmHg subsequent to histamine infusion.

Compliance estimation. Figure A-8 illustrates the change in EVF resulting from a change in effective microvascular driving pressure in both control and the SVCP elevation groups. When LAP was elevated above control, a greater amount of pulmonary fluid accumulated in animals with elevated SVCP levels than the control group with normal SVCP. The estimate of Edemagenic Gain of the SVCP elevation group is 0.069

ml/g·mmHg, and that of the control group is 0.018 ml/g·mmHg. Assuming a high R_L (Fig. A-8B), the interstitial compliance of the SVCP elevation group is therefore 0.069 ml/g·mmHg.

Comparison between effects of histamine and endotoxin infusion. Figure A-8 illustrates the change in EVF in response to a change in effective microvascular driving pressure in the control case, as well as with histamine infusion, endotoxin infusion, and SVCP elevation. Edemagenic Gain was the lowest in the control case (0.018 ml/g·mmHg). Edemagenic Gain of the endotoxin group (0.112 ml/g·mmHg) was greater than the histamine (0.04 ml/g·mmHg) and SVCP elevation groups (0.069 ml/g·mmHg).

5. VENOMOTION MODULATES LYMPHATIC PUMPING IN THE BAT WING

5.1 METHODS

Bat preparation. Experimental procedures and animal care were performed in compliance with the Texas A&M University Institutional Animal Care and Use Committee. With a few notable exceptions, experimental procedures were similar to those employed by Widmer et al. (152, 153). Briefly, Pallid bats (n=8) were maintained in a colony for over two years before experimentation. Bats were trained to participate in experiments without anesthesia, lying in a plastic box with their wing extended outside of the box. Following an established schedule, no bats were used for experimentation more than once per week, and no experiment lasted more than six hours. Bats were placed in a plastic box attached to a temperature-controlled glass plate (Olympus Tokai Hit) set at 27°C. The vasculature was visualized with an intravital microscope (Olympus BX61WI) utilizing a water-immersion lens at 400X magnification, and the image was recorded at 30 frames per second via digital video recorder (Panasonic KR222 S-Video Camera). Custom video caliper software was developed (LabView 7.1) to quantify vascular diameters from video recorded at 30 Hz.

Vessel selection. The relative position of venules and lymphatic vessels was similar in all bats (Fig. A-9). The location selected for study was upstream of the first arteriolar bifurcation between the third and fourth phalanges. Venules at this location averaged 90-110 μm in diameter and were located between arterioles and lymphatic microvessels. Only spontaneously contracting lymphatic microvessels (12-25 μm

diameter) adjacent to venules were studied. At the selected location, the video was recorded for at least 5 minutes to ensure a stable baseline (152, 153).

Procedures for correlating venomotion and lymphatic vessel contraction. Two sets of experiments were conducted. In the first set of experiments, the role of naturally existing venomotion in lymphatic pumping was evaluated without any particular intervention. For each venomotion cycle, peak diastolic and systolic venular diameters (D_V) as well as corresponding lymphatic microvascular diameters (D_L) were simultaneously recorded as a function of time. From these data, critical values were derived, including frequency of venular contraction (f_V), frequency of lymphatic contraction (f_L), magnitude of diameter change for each venomotion cycle (ΔD_V), the rate of change of venous diameter during the venomotion cycle ($\mathrm{d}D_V/\mathrm{d}t$), and the time delay ($\Delta t$) between peak systolic venular diameter and the beginning of lymphatic vessel contraction. For each cycle, the venomotion period (T) was determined from the time between two consecutive venular dilations. Cross-sectional area (A_L) of lymphatic microvessels was calculated from measured diameter (D_L) assuming a cylindrical conformation. To evaluate effectiveness of the extrinsic expansion and compression of the lymphatic microvessel by venomotion, only passive changes in the cross-sectional area were considered. Changes in lymphatic microvascular cross-sectional area due to active contraction were neglected. Active change in lymphatic microvascular diameter was distinguished from passive change by tracking the walls of the lymphatic microvessel. Walls moved towards each other during active contraction.

Procedures to abolish venomotion. In the second set of experiments, the causal relationship between venomotion and lymphatic microvascular contractions was evaluated by abolishing venomotion. Davis et al. previously reported that an increase in venular transmural pressure dilated venules and abolished venomotion (30). In the present study, venular transmural pressure was increased and venomotion was abolished by completely occluding the venules downstream from the point of observation. Venules were selectively occluded using blunt glass micropipettes to compress the venules against the glass plate under the wing. Lymphatic microvessel contraction frequency before and after selective venular occlusion (with a two minute equilibration period) were compared.

Linear regressions and *t*-tests were performed using a statistics software package (SAS Institute, Inc.). A p value less than 0.05 was considered significant.

5.2 RESULTS

To characterize the topology of the lymphatic network, lymphatic microvessels adjacent to venules with diameter > 40 μm (exhibiting venomotion) were traced to venules with diameter < 25 μm (not exhibiting venomotion). In each experimental subject, lymphatic microvessels were paired with venules exhibiting venomotion. However, lymphatic microvessels were found to cross over and become paired with adjacent arterioles when venules were too small to exhibit venomotion (diameters < 25 μm).

Figure A-10 depicts the peak systolic and peak diastolic venular diameters of a representative venule exhibiting venomotion and the passive change in the adjacent lymphatic vessel diameter. Discontinuities in the illustrated lymphatic vessel diameter correspond to the active change in diameter due to intrinsic contraction. The oscillation of venular diameter exhibits a natural variation in the magnitude as well as the frequency. This natural variation in venomotion allowed correlation of changes in venular diameter to changes in lymphatic diameters without requiring a particular intervention. Diameters of a representative venule and an adjacent lymphatic microvessel are illustrated in Fig. A-11 to indicate critical time points such as Δt (the time from c to d, Fig. A-11) and T (the time from b to b, Fig. A-11).

Figure A-12 indicates the percent passive change in lymphatic microvascular cross-sectional area. A 58.5±15% change in cross-sectional areas of lymphatic microvessels was observed as adjacent venules dilated and contracted in the absence of active lymphatic contraction. This change in cross-sectional area compares to a ~67% change in cross-sectional area of the lymphatic microvessels due to active contractions of lymphatic microvessels reported by Benoit et al (7).

Next the impact of spontaneous venular contractions on active lymphatic contractions was characterized. The distribution of the number of lymphatic microvascular contractions occurring after the onset of venous contraction expressed relative to the venomotion period (Fig. A-13) illustrates that the lymphatic microvascular contractions were correlated with venular activity (i.e. with venular dilation as well as contraction). In fact, 86% of lymphatic microvascular contractions occurred in the first

half of the venomotion period. Time point C in Fig. A-13 corresponds to the peak venular systole (occurring within the first 20.99±6% of the venomotion period).

Figure A-14 illustrates the relationship between lymphatic microvascular contraction frequency and venomotion frequency. The slopes obtained from the linear regression of individual data sets indicated that venomotion frequency and lymphatic microvascular contraction frequency were positively correlated (one-sample *t*-test, $p<0.001$).

The lymphatic muscle response was observed to vary with the magnitude and velocity of venomotion. Figure A-15 illustrates the time delay (Δt) between peak venular systole and the beginning of lymphatic vessel contraction as a function of magnitude and velocity of venomotion. With increased magnitude of venomotion, the time delay (Δt) before the onset of lymphatic contraction was significantly reduced (one-sample *t*-test, $p<0.001$, Figs. A-15A and B). As the velocity of venomotion increased, the time delay (Δt) was significantly reduced (one-sample *t*-test, $p<0.001$, Figs. A-15C and D). In one notable exception (*vessel 7*, Figs. A-15B and D), the association of magnitude as well as velocity of venomotion with the time delay was not evident, even though the lymphatic microvascular contraction frequency was positively correlated with venomotion frequency. This case was unusual because the lymphatic microvessel contracted at a much higher rate than the other vessels, and a relatively large percentage (35%) of its contractions occurred during the last 70% of the venomotion period.

Complete occlusion of the venules downstream from the observation point abolished venomotion in accord with a previously reported study (30). Figure A-16A

depicts the diameter of a representative venule before and after the complete occlusion of the venule downstream from the point of observation. Figure A-16B illustrates the distribution of lymphatic contractions before and after the venular occlusion. A 54.3±20% decrease in lymphatic contraction frequency was observed when venomotion was abolished ($p<0.001$).

6. DISCUSSION AND CONCLUSIONS*

6.1 SPECIFIC AIM 1

The present work provides the first algebraic characterization of interstitial fluid balance resulting from the interaction of microvascular, interstitial and lymphatic function. This novel theoretical framework addresses several limitations inherent in conventional quantitative approaches (40). First, by allowing interstitial fluid pressure (P_i) and protein concentration (C_i) to vary with interstitial inflow and outflow, the present analysis requires a minimal number of assumptions. Most notably, P_i and C_i were not assumed constant (40), but were formulated in terms of microvascular and lymphatic parameters (*Eq. 3.8*). Second, by exploiting an existing algebraic description of the lymphatic system (38), this novel formulation does not neglect the feedback provided by lymphatic function. That is, while other reports are limited to the effect of interstitial fluid pressure on lymphatic function (7, 106), this work includes the effect of lymphatic function on interstitial fluid pressure. Third, this approach goes beyond describing interstitial fluid balance only in terms of conservation of mass, by introducing the concept of inflow and outflow resistances (Fig. A-3). The reciprocal of the microvascular filtration coefficient ($1/K_f$) is revealed to be an inflow resistance, a natural counterpart to the effective lymphatic resistance (R_L).

Fourth, the resulting approach reveals that steady-state interstitial fluid pressure depends on a simple ratio of $1/K_f$ and R_L. Surprisingly, interstitial compliance has no effect on steady-state interstitial fluid pressure. Fifth, since the results can be represented by algebraic equations, the present work provides a general solution in terms of physiologically-relevant parameters. Unlike published results of numerical simulations which assume very specific values of parameters (12, 13, 22, 70, 71, 129, 166), the present solution can be easily customized to represent a particular experimental condition without resorting to solving differential equations. Sixth, this approach applies the familiar balance point concept (62, 67) to characterize interstitial fluid balance. The resulting graphical approach (Fig. A-4) provides a novel means to conceptualize the complex process of fluid balance without having to contemplate the interaction of eight separate equations (*Eqs. 3.2-3.7*). Taken together, the present work develops a novel theoretical framework that yields critical insights into the complex interaction of microvascular, interstitial, and lymphatic function.

Algebraic formulation of interstitial fluid volume and protein regulation. Unlike conventional approaches that require numerical solutions (12, 13, 22, 70, 71, 129, 166), the present work derived a series of simple algebraic formulas characterizing interstitial fluid volume and protein regulation. The resulting approach integrated simplified equations (*Eqs. 3.2-3.7*) that characterize the microvasculature, interstitium, and lymphatic system using the classical control theory concepts of linearity and time invariance (34, 49). The benefits of this approach are fourfold. First, the resulting block-diagram (Fig. A-1) promotes intuitive understanding of the interrelations between

subsystems. Second, this approach aids experimental design by separating parameters that characterize the system (σ, K_f, R_L, and C) from variables that are experimentally manipulated or measured (P_c, C_c, P_{out}, P_i and C_i). Third, the resulting algebraic solutions can be easily customized for different organs by altering parameter values. Fourth, the simple results embodied in *Eq. 3.8* provide a level of conceptual clarity that leads to new insights. For instance, it is evident that interstitial compliance has no effect on steady-state interstitial fluid pressure. *Equation 3.8* provides a new tool for physiologists to study the physics of interstitial fluid balance. None of these four benefits can be realized via conventional approaches that require numerical solutions.

Reconceptualizing interstitial fluid balance with inflow and outflow resistances. A singular benefit of expressing interstitial fluid pressure with an algebraic function is that it leads to a new framework to understand interstitial fluid balance. Reformulating the equations describing microvascular filtration as a transfer function (34, 49) relating a microvascular driving pressure ($[(P_c-P_i)-\alpha\sigma\,(C_c-C_i)]$) to an inlet flow ($J_v$) results in an effective resistance to microvascular filtration equal to $1/K_f$. Similarly, Drake et al. (38) characterized lymphatic drainage as a transfer function relating a lymphatic driving pressure ($P_i+P_p-P_{out}$) to an outlet flow (J_L), resulting in an effective lymphatic resistance (R_L) (*Eq. 3.3*). When combined, these transfer functions suggest an electrical circuit analogy consisting of two resistances in series (Fig. A-3A). Three new concepts are generated by this electrical analogy. First, the ratio of R_L and $1/K_f$ determines interstitial fluid pressure (Fig. A-3A). In fact, the relative values of R_L and $1/K_f$ determine whether P_i approaches the effective microvascular driving pressure (when $R_L>1/K_f$) or effective

lymphatic pumping pressure (when $R_L<1/K_f$). Second, the sum of R_L and $1/K_f$ determines the total resistance and thus lymph flow. Interstitial fluid pressure and lymph flow can therefore be regulated independently. Third, there is a natural analogy to regulation of capillary pressure (Fig. A-3B). Notably, capillary pressure also results from the ratio of inflow (arteriolar) and outflow (venular) resistances, and is unaffected by (capillary) compliance (120).

Steady-state interstitial fluid pressure is not affected by interstitial compliance. The belief that interstitial compliance affects interstitial fluid pressure can be traced to the original work of Guyton et al. (63). Clearly, interstitial compliance by definition relates a *change* in interstitial fluid volume to a *change* in interstitial fluid pressure. However, the present work reveals that the *absolute value* of interstitial fluid pressure in steady state is not affected by interstitial compliance (*Eq. 3.8a*). Instead, steady-state interstitial fluid pressure is only a function of the resistances to interstitial fluid flow ($1/K_f$ and R_L) and driving pressures ($[P_c-\alpha\sigma\ (C_c-C_i)]$ and $[P_{out}-P_p]$) (Fig. A-3). The irrelevance of interstitial compliance to interstitial fluid pressure is illustrated by a series of experiments in which interstitial compliance is experimentally increased by infusing inflammatory agents or inducing trauma (132). Although the significant increase in interstitial fluid volume was sustained, the interstitial fluid pressure eventually approached baseline values (99, 132). Small persistent deviations from baseline values may have been the result of confounding alterations in microvascular permeability (4, 108, 132). Once interstitial fluid pressure is determined by the ratio of inflow and outflow resistances, interstitial storage capacity, characterized by the interstitial fluid

volume-pressure relationship, determines the corresponding interstitial fluid volume (Fig. A-2A). Nonetheless, interstitial compliance is a critical parameter that affects the susceptibility of an organ to edema formation, characterized by the concept of Edemagenic Gain (34).

Validity of assumptions. To arrive at the simple algebraic solutions in the present work (*Eq. 3.8*), a number of assumptions were required. The first set included assumptions that are commonly made when modeling microvascular filtration. Focusing on whole-organ fluid balance, the common assumption was made that the interstitial space within an organ behaves as a well mixed compartment—there is no concentration gradient across interstitial space (147). This assumption may result in an overestimation of the flow of fluid and proteins across microvascular membrane when microvascular filtration is low (147). Although several equations are reported that describe microvascular protein extravasation, the Taylor-Granger Equation (*Eq. 3.3*) was selected, because it is relatively simple and has been experimentally validated (147). This equation tends to overestimate microvascular protein extravasation when microvascular filtration is low, but approaches the well-accepted nonlinear Patlak-Hoffman formulation (123) with increasing microvascular filtration (see *Appendix C*). A less-common set of assumptions is required specifically for the present work. Although all variables characterizing microvascular, interstitial, and lymphatic function have nonlinear relationships, for conceptual clarity they were represented with linear relationships (*Eqs. 3.2-3.7*). Linearization incurs minimal error if either the variables vary within a small range, or the relationships are treated as piecewise linear (12, 22,

70). The interstitial fluid volume-pressure relationship is particularly nonlinear, since the slope increases dramatically at higher hydration levels (63). This particular nonlinearity has minimal impact in the present work, because interstitial compliance has no effect on steady-state interstitial fluid pressure (*Eq. 3.8a*). Another critical assumption of linearity is embodied by the description of lymphatic function, appropriated from Drake et al. (38). Two critical parameters, R_L and P_p, were derived empirically, and represent the slope and intercept of the lymphatic outflow-pressure relationship. As has been argued previously(6), R_L and P_p do not represent the physical resistance to lymph flow or the pressure developed by lymphatic contractions. Recently, R_L and P_p have been revealed to be related to both lymphatic vessel contractility and contraction frequency (126). Also, parameters characterizing microvascular filtration are typically reported in units per weight. Because lymphatic parameters characterize whole-organ behavior, they must be normalized to make their units consistent. Finally, to illustrate the ability of the resulting equations (*Eq. 3.8*) to predict interstitial fluid pressure and protein concentration, specific parameter values had to be assumed (Table B-1). Because the parameter values reported from the literature resulted from different animal models, organ systems, and experimental interventions, their range were relatively large. In the end analysis, however, the fact that predicted values compared favorably to measured values provides the greatest argument for the validity of the assumptions used in the present work.

Graphical balance point approach permits intuitive conceptualization of complex problems. The algebraic solutions developed in the present work (*Eq. 3.8*) are manifestations of a balance-point characterization of interstitial fluid volume and protein

regulation. Like Guyton, who used a balance point approach to characterize heart-arterial interaction resulting from an equilibrium between venous return and cardiac output (62, 67), microvascular-lymphatic interaction resulting from an equilibrium between the inflow and outflow of fluid and proteins (Figs. A-1A and B) is characterized in the present work. Although numerical approaches to solve the interstitial fluid flow equations are powerful enough to include even relatively unimportant details, the graphical balance point approach derived from *Eq. 3.8* is simple enough to reveal fundamental behaviors. For instance, the graphical balance point approach can be used to quickly identify the effect of changing any one parameter on interstitial fluid pressure and lymph flow. Figure A-4A illustrates that increasing K_f shifts the balance point (from A to B), yielding higher interstitial fluid pressure and lymph flow. Figure A-4B illustrates that increasing R_L shifts the balance point, yielding higher interstitial fluid pressure and lower microvascular filtration. Figure A-4C illustrates that increasing capillary pressure (P_c) shifts the balance point, yielding higher interstitial fluid pressure and lymph flow. Figure A-4D illustrates that increasing lymphatic outlet pressure (P_{out}) shifts the balance point, yielding higher interstitial fluid pressure and lower microvascular filtration. Perhaps more importantly, this graphical approach can reveal surprising behavior resulting from the interaction of parameters. For instance, although simultaneous increase in K_f and R_L (shifting the balance point from A to B in Fig. A-4E) will yield higher interstitial fluid pressure and thus volume, microvascular filtration and lymph flow can remain unchanged. The common practice of using lymph flow to estimate K_f (40) may therefore fail. Conversely, an increase in K_f, if accompanied by a

decrease in R_L, (shifting the balance point from A to B in Fig. A-4F) will yield increased microvascular and lymphatic flow without a corresponding change in interstitial fluid pressure. In fact, interstitial fluid volume would remain unchanged. Use of gravimetric approaches to infer changes in K_f (40) would therefore fail. These simple examples illustrate how this novel graphical approach can be used in the basic sciences to challenge established scientific techniques, in the clinical sciences to explore new ways to compensate for changes in properties such as increases in microvascular permeability (Fig. A-4A), and in education to introduce new students familiar with the balance point concept to integrated interstitial fluid balance. The ultimate contribution of the present work, however, may be that it provides a powerful analytical tool, yet is relatively simple to use.

6.2 SPECIFIC AIM 2

A new concept has been developed, referred to as "Edemagenic Gain", relating changes in effective microvascular driving pressure to changes in interstitial fluid volume, and related to the three most important phenomena affecting fluid balance—microvascular filtration, lymphatic function, and interstitial fluid storage capacity (*Eq. 4.3*). By making simplifying assumptions, it was possible to derive a simple algebraic formula for Edemagenic Gain. The resulting first-order approximation was rearranged to separate parameters characterizing structure (i.e., microvascular permeability, effective lymphatic resistance, and interstitial compliance) from input and output variables characterizing function (i.e., change in effective microvascular driving pressure and

change in interstitial fluid volume). The resulting formulation presents the solution to classical fluid balance equations in a form recognizable as a classical negative feedback system (Fig. A-6A). Thus, by accepting the cost of losing a degree of accuracy, the benefit of conceptual clarity can be reaped that is not currently available from complex numerical simulations.

The concept of gain as an integrational approach to interstitial fluid dynamics. Mathematically modeling the dynamics of interstitial fluid balance has had a long history, (12, 13, 22, 64, 70, 71, 129, 166) and resulted in concepts such an edema "safety factor" that have played a significant role in our current understanding of edema formation (66). Typically, these approaches focused solely on hemodilution or hemorrhage, and the role of vascular permeability. Given how often the concepts of vascular permeability and interstitial compliance are invoked, it is perhaps overlooked that K_f is a "black box" parameter relating hydrostatic and colloid osmotic pressure gradients to microvascular filtration and that C is a "black box" parameter relating interstitial fluid volume to pressure. The "black box" approach to interstitial fluid balance has further been refined. K_f, for instance, has been further reduced into smaller black boxes, such as "hydraulic conductivity" and "surface area" (109, 110). The introduction of molecular biology analytical techniques has provided further opportunities to provide mechanistic interpretations, especially in the understanding of changes in interstitial compliance (128, 132). Although this process of reductionism has led to fundamental new understanding of the individual physiological processes involved in edema formation and resolution, it has been unclear how these mechanistic elements

interact with each other and thus affect interstitial fluid volume as a global variable, the necessary step to bridge basic science to clinically-relevant research. The approach used in the present work therefore provides an integrational approach that complements reductionist approaches, providing the means to 1) predict the implications of changes in any of the currently identified mechanistic elements on interstitial fluid volume, 2) determine the dominant mechanisms that have the greatest impact on interstitial fluid volume, 3) identify which parameters must first be determined before ascribing edema formation to any one process. Our integrational approach is complementary to mechanistic studies, and in the present case, has at least identified what remains unknown and requires further study.

Necessary components to describe a physiological process as a gain. In order to derive an algebraic formula that characterizes a complex physiological process in terms of a constant "gain", it is necessary to formulate the system as 1) linear, 2) first-order, and 3) time-invariant (49, 89). Even though most physiological processes are highly nonlinear, approximating them as linear is permissible when changes in the variables of interest are small. When variables change sufficiently to make nonlinear effects significant, it is common practice to treat the system as "piecewise linear". For example, the interstitial fluid pressure-volume relationship can be approximated as a combination of two linear relationships corresponding to two different levels of hydration (12, 22, 70). Similarly, although most physiological processes can be overwhelmingly complex, approximating them as first-order (i.e., eliminating secondary effects) is permissible when the secondary effects are small. For instance, to arrive at the relationship between

lymphatic driving pressure and lymph flow in Drake-Laine formulation (38), reabsorption of the lymphatic fluid back into circulation in lymph nodes is neglected. The final criterion, time-invariance, requires that all parameters except the input and output variables (i.e., interstitial fluid volume and microvascular pressure) have constant values. That is, parameters such as C, R_L, K_f and σ are relatively constant, and do not vary appreciably from moment to moment. If any particular intervention alters one of these parameters, then the gain is said to have changed. Taken together, the assumptions that the system is linear, first-order, and time-invariant make it possible to avoid using a highly complex convection-diffusion transport model which must be solved numerically. Although numerical solutions can include many relevant details (12, 13, 22, 70, 71, 129, 166), they cannot be expressed as a simple algebraic formula. In fact, such solutions can only be plotted graphically. Plotting volume as a function of just four parameters (C, R_L, K_f and σ) cannot be accomplished in a single graph. Numerical solutions thus suffer from a loss of conceptual clarity, since they lack an explicit relationship of cause and effect, and require the knowledge of numerous variables that cannot be retrieved experimentally.

Reinterpreting the Lymphatic "Effective Resistance". The Drake-Laine lymphatic system model characterizes the lymphatic flow as a function of two lumped parameters: one describing the slope of the pressure-flow relationship and one describing the intercept. Using a convenient analogy to an electric circuit, these quantities have been referred as "effective lymphatic resistance" (R_L) and "lymphatic pump pressure" (P_p). Values for these parameters have not yet been predicted from first principles, but

are estimated from linear regression of measured data. They are therefore empirical (descriptive) parameters (38). To date R_L and P_p have been used to describe lymphatic function in a number of organs (39, 42, 44, 91, 93), but have yet to be assigned particular physiological interpretations. Much like K_f, a "black box" parameter relating hydrostatic and colloid osmotic pressure gradients to microvascular filtration and C, a "black box" parameter relating interstitial fluid volume to pressure, R_L and P_p are similar "black box" parameters which relate lymphatic outflow to interstitial fluid pressure. Since transserosal flow, flow across the serous membrane which encloses several organs, is ultimately collected by lymphatics and returned to systemic circulation, transserosal flow is accommodated by the Drake-Laine model. The historical use of the term "effective resistance" to describe the empirically-derived slope of the line of the pressure gradient-flow relationship is unfortunate and has caused some consternation, since this empirical relationship clearly arises from an active pumping of lymph, rather than a purely passive process as implied by the term "resistance" (6).

Edemagenic Gain suggests a novel structure-based classification of edema. The equation used in the present work to approximate Edemagenic Gain (*Eq. 4.3*) assumes an even simpler form (*Eq. 4.4*) when specific parameters are either very large or small. In the first case, when effective lymphatic resistance is significantly elevated, $R_L \cdot K_f$ can become much larger than 1. The value of $1+R_L \cdot K_f$ thus becomes approximately equal to $R_L \cdot K_f$ and EG can be approximated by C. Under such conditions, interstitial compliance alone determines Edemagenic Gain and thus the susceptibility to edema, irrespective of the particular value of the microvascular filtration coefficient (Fig. A-6B). In other

words, Edemagenic Gain becomes "Compliance-Dominated". In most other cases, however, R_L is relatively small, including edema caused by enhanced microvascular permeability. Edemagenic Gain then depends on the combination of interstitial compliance (C), effective lymphatic resistance (R_L), and microvascular permeability (K_f) (Fig. A-6B). In this case, Edemagenic Gain is "Multivariate". This analysis has therefore revealed two types of gain; "Compliance-Dominated" approximately equal to C and "Multivariate" dependent on C, R_L and K_f. In both cases, interstitial compliance plays a significant role in edema formation. This structure-based classification of edema provides a novel approach to estimate interstitial compliance on one hand, and a novel insight into the causes of edema on the other.

Edemagenic Gain provides a novel approach to estimate interstitial compliance. Conventional techniques to estimate interstitial compliance require recording changes in both interstitial fluid volume and interstitial hydrostatic pressure. Whereas methods to measure changes in tissue fluid volume are fairly accurate and stable, measuring interstitial hydrostatic pressure is problematic. Wiig et al. reported significant deviation when comparing interstitial hydrostatic pressure measurements derived from micropipette techniques, chronic perforated and porous capsule techniques, and wick methods (159-162). The concept of Edemagenic Gain provides an alternative approach that eliminates the need to measure interstitial fluid pressure. By increasing effective lymphatic resistance (or alternatively increasing lymphatic outlet pressure), Edemagenic Gain becomes equal to interstitial compliance (C) (*Eq. 4.4*). Only changes in interstitial fluid volume and microvascular hydrostatic pressure therefore must be measured to

estimate *C*. This method can be particularly useful to determine chronic changes in tissue compliance, especially in the myocardium and lungs where interstitial fluid pressure measurement is confounded by tissue motion (113). Indeed, since the edema in the SVCP elevation group described in Fig. A-8 was caused by an intervention that decreased lymphatic flow (comparable to impaired outflow edema), Edemagenic Gain is expected to depend only on the interstitial compliance (Fig. A-6B). Interstitial compliance estimated using our novel method (C = 0.069 ml/g·mmHg) is within the range previously estimated by conventional methods (Table B-2).

Edemagenic Gain provides a novel insight into the causes of edema. Determining how a physiologic intervention causes edema is particularly difficult, because it is not possible to directly measure microvascular permeability, effective lymphatic resistance, and interstitial compliance in a single experiment. The present work uses the example of histamine-induced edema to illustrate how the concept of Edemagenic Gain can reconcile disparate reports. First, several reports suggest that increases in the microvascular filtration coefficient are responsible for histamine-induced edema (11, 88, 108, 115, 124). Second, inhibition of lymph flow by histamine (47, 127), suggests changes in lymphatic function could be responsible for histamine-induced edema. Third, interstitial fluid pressure measurement studies have demonstrated that interstitial compliance increases significantly after histamine infusion, suggesting changes in compliance alone may be responsible for histamine-induced edema, as it is for edema induced by other inflammatory agents (3, 9, 10, 57, 83, 86, 87, 119, 130, 134, 164). From an experimental standpoint, our results (slope, Fig. A-7) clearly indicate that

histamine increases Edemagenic Gain by approximately a factor of two. However, our theoretical formulation (*Eq. 4.3*) suggests that all three parameters C, R_L and K_f may determine the extent of edema formation. In this case, there is not enough information contained in the data to exclude any of the three postulated edemagenic mechanisms.

Active regulation of C, R_L and K_f. Until recently, interstitial compliance and effective lymphatic resistance were considered as passive properties (63, 66). Recent studies, however, have suggested that these properties are actively regulated. Effective lymphatic resistance, for instance, has been shown to be a regulated property, since it is affected by several neurohormonal factors that modulate lymphatic function (46, 47, 73, 76, 127, 146). Furthermore recent studies have suggested that interstitial compliance is not only passively affected by the level of hydration, but also by modulation of β1-integrin adhesions (87, 128, 132, 163, 165). The present work presents a framework to study the effect of acute to chronic regulation of the structural properties C, R_L and K_f. Not only can the Edemagenic Gain be used to identify changes in critical properties that produce edema, such as permeability, it can conversely identify structural changes resulting from edema, such as changes in interstitial compliance following fibrosis.

Generalizing Edemagenic Gain: incorporating changes in σ and Π_i. In the formulation of Edemagenic Gain given by *Eq. 4.3*, only three parameters, C, R_L and K_f, determine the relationship between the change in effective microvascular driving pressure and the change in interstitial fluid volume. In this particular formulation of Edemagenic Gain, there are two constants: the microvascular reflection coefficient (σ), which characterizes the relative microvascular permeability to proteins, and interstitial

colloid osmotic pressure (Π_i). Changes in the reflection coefficient as well as interstitial colloid osmotic pressure, however, can affect interstitial fluid volume. The values of σ and Π_i were not determined in the present study, although there is evidence that histamine and endotoxin decrease σ and may increase Π_i (19, 53, 108, 124). To take advantage of measurements of σ and Π_i in future studies, Edemagenic Gain could be reformulated (see *Appendix D*) such that σ and Π_i are variables (*Eq. A6*). In this case, the Edemagenic Gain is expressed as $\Delta V/\Delta(P_c\text{-}\sigma\cdot(\Pi_c–\Pi_i))$. Not only can this more general formulation incorporate changes in σ or Π_i, it can capture such phenomena as "protein washdown". This more general formulation degenerates into $\Delta V/\Delta(P_c\text{-}\sigma\cdot\Pi_c)$, as in *Eq. 4.3*, when variables σ and Π_i are constant. If all the parameters change (e.g., P_c, Π_c, Π_i and σ) with a particular intervention, then they would all need to be independently measured. The measurement of σ and Π_i would allow more accurate estimation of the Edemagenic Gain. The process of simplification used in the present work could therefore be used as a guide for investigators developing new approximations of Edemagenic Gain. Caution is advised, however, a previous attempt to relate interstitial volume to effective microvascular driving pressures (53) oversimplified the equations, and the critical contribution of interstitial compliance was neglected (see *Appendix D*).

Extrapolation of Edemagenic Gain estimations to different organs. The Edemagenic Gain formulation is general—no assumptions of a specific organ or parameter values were necessary to define EG in *Eq. 4.3*. To use the Edemagenic Gain formulation for a specific organ, the model should be evaluated and validated with

particular attention to the specific assumptions made for the organ under study. In the present study, for instance, values of C, R_L and K_f listed in Table B-2 are used to characterize interstitial fluid balance in lung. The lung model has been well-studied over the last four decades, and the measurements for all three parameters (C, R_L and K_f) have been determined (Table B-2). A dilemma may arise, however, when extrapolating the outcomes to other organ systems, especially those for which the measurements of the parameters are not available. In this case, either the unknown parameters must be determined before predicting the Edemagenic Gain, or the ranges of the permissible values of the parameters should be determined to estimate the range of Edemagenic Gain that can result. The sensitivity analysis presented in Table B-3 provides some guidance to determine how critical a particular parameter value is. In some specific cases (such as when the Edemagenic Gain is "Compliance-Dominated"), the particular values of parameters (such as R_L and K_f) have a relatively small influence. Extrapolation of the present model implementation to other organ systems must be evaluated on a case-by-case basis.

Inflammatory agents have disparate effects on Edemagenic Gain. The concept of Edemagenic Gain can be used to characterize the extent to which specific inflammatory agents can sensitize tissues to edemagenic conditions. Both histamine and endotoxin are pro-inflammatory agents that can result in similar degrees of edema. However, pulmonary edema induced by endotoxin does not regress, even after significant reduction in effective lymphatic resistance (92). Analysis presented in Fig. A-8 provides a potential interpretation. The endotoxin group has a larger Edemagenic Gain (0.112

ml/g·mmHg) than either the histamine group (0.034 ml/g·mmHg) or the superior vena caval pressure elevation group (0.069 ml/g·mmHg). The endotoxin group is therefore approximately twice as sensitive to changes in effective microvascular driving pressure. Although these results are likely dose-dependent, this particular example suggests that endotoxin-induced edema is potentially more serious, less stable, and more likely to present as acutely fulminating edema. The concept of Edemagenic Gain does not provide a measure of edema, but instead provides an index of an organ's susceptibility to edema formation.

6.3 SPECIFIC AIM 3

The present work demonstrates that venomotion modulates the pumping of lymph by both compressing adjacent lymphatic microvessels (32) and mechanically triggering intrinsic lymphatic contractions. First, venous dilation and contraction produced a significant change in lymphatic microvascular cross-sectional area. Second, lymphatic microvascular contractions were immediately preceded by a change in venular diameter (Fig. A-13). Third, venular and lymphatic vessel contraction frequencies were correlated (Fig. A-14). Fourth, the time delay between the peak venular systole and the onset of lymphatic microvascular contraction was negatively correlated with venomotion magnitude and velocity (Fig. A-15). Fifth, lymphatic microvessels are paired with venules that exhibit marked venomotion, but with arterioles when adjacent venules lack venomotion. Sixth, a decrease in lymphatic contraction frequency was observed when venomotion was abolished (Fig. A-16). Taken together, these pieces of evidence are

consistent with both extrinsic pumping of lymph by venules and mechanical triggering of intrinsic lymphatic contractions. These results also imply that with venular-lymphatic coupling, extrinsic and intrinsic lymph pumping mechanisms not only coexist, but also are coupled.

Evidence of mechanical origin of venule-lymphatic coupling. The possibility that venular and lymphatic contractions are both initiated by a common neural, electrical, or humoral factor must be addressed. First, venules as well as lymphatic microvessels in bats are not innervated (25, 82, 155). If each pair of venules and lymphatic microvessels was jointly innervated in the bat wing, there would have to be a consistent delay before the initiation of lymphatic contraction. Second, there is no apparent connection between the muscular layers of venules and lymphatic microvessels to provide direct electrical conduction. Furthermore, there is not a one-to-one coordination of lymphangion and venular contraction cycles (Fig. A-14) that would be expected to accompany direct electrical conduction. With regard to the diffusion of a humoral factor, the diffusion distance for humoral factors to travel from venules to lymphangions (~30 microns) is too large for the small time delay (0.6 sec, 10% of the venomotion period) between venular and lymphatic contraction (Fig. A-13). None of these non-mechanical factors are consistent with all six observations presented above. In contrast, all six observations are consistent with the well-established phenomena of stretch-induced vascular muscle contraction (116).

Abolishing venomotion to modulate lymphatic contraction. To ensure that the correlation of lymphatic vessel contraction with venomotion is causal and mediated by

mechanical stimulation, a mechanical intervention was required. It was not possible to establish causality by abolishing venomotion pharmacologically without incidentally inhibiting lymphangion contraction. The close proximity of the lymphatic microvessels to venules made it impossible to independently dose venules with drugs (e.g., calcium channel blockers). However, Davis et al. previously reported that raising venular transmural pressure abolishes venomotion in the bat wing (30). Therefore the venules were selectively occluded to raise their transmural pressures. Although, venular transmural pressures were not measured, the occlusion produced venular dilation and abolished venomotion. It is possible that in the process of occluding some venules, the adjacent lymphatic vessels may have been occluded. However, a previously reported increase in the lymphatic contraction frequency with elevated lymphatic transmural pressure (7, 75, 106) was not observed in any of the vessels in the present study (Fig. A-16). The reduced lymphatic microvascular contraction frequency associated with abolished venomotion provides evidence that venomotion mechanically stimulates intrinsic contractions of adjacent lymphatic microvessels.

Methodological challenges to quantifying relative contribution of extrinsic pumping. There are a number of notable methodological limitations particular to our unique animal model. First, only lymphatic microvessels that exhibited spontaneous contraction were studied, since they could be identified without the use of contrast agents that might affect lymphatic function (2). Although the selection of only these vessels introduces a selection bias, the result would be to underestimate the relative role of extrinsic pumping on lymph propulsion. Second, it was not possible to visualize the

entire length of a lymphangion while making accurate diameter measurements. It is therefore possible that compression of a lymphangion segment does not propel lymph through downstream valves, but merely acts to passively expand the portion of lymphangion outside the field of view. However, the observed percent change in lymphangion cross-sectional area caused by venomotion was comparable to the observed percent change in lymphangion cross-sectional area (67%) caused by intrinsic contraction reported by Benoit et al. (7) (Fig. A-12). Third, since the Pallid bats were lightly restrained, did not move during experiments, and have wings devoid of skeletal muscle, the only source of extrinsic compression of lymphangions arose from venomotion. Stresses within the wing membrane during flight, however, may provide another source of extrinsic propulsion of lymph. Fourth, the bat wing was not exposed to edemagenic challenges known to increase interstitial fluid pressure. The relative contribution of venomotion to lymph propulsion therefore may decrease when lymphangions are stimulated to contract with a greater force or with a greater frequency. Nonetheless, the 58.5±15% change in lymphangion cross-sectional area suggests that extrinsic propulsion of lymph due to venomotion plays as great a role as intrinsic lymphangion contraction in the normal resting state.

Increasing effectiveness of lymph propulsion in the face of an edemagenic challenge. This is the first work to offer evidence of coordination between intrinsic and extrinsic pumping of lymph. Such coordination may simply increase the efficiency of lymph propulsion. However, such coordination may also increase the effectiveness of lymphangion pumping in the face of an edemagenic challenge. The ability of

lymphangions to propel lymph depends on their contractility, diastolic function, preload, and afterload (7). Lymphatic microvascular compression due to venular expansion could enhance lymphatic microvascular contractility, increasing the "effective inotropy". Similarly, lymphatic microvascular expansion due to venular contraction could facilitate faster lymphatic microvascular filling, increasing the "effective lusitropy". In addition, venular compression of an upstream lymphangion may increase preload, and venular expansion of a downstream lymphangion may decrease afterload. Because these four behaviors can enhance the intrinsic lymph pump, venomotion may act as a previously unidentified anti-edema mechanism. For instance, locally heating the skin not only leads to greater microvascular filtration, but also increased venomotion magnitude, velocity, and frequency and thus possibly enhanced lymphatic function (15, 85). In fact, any phenomena that increase capillary and venular pressures can increase both microvascular flux and venomotion (30, 158).

Implications for lymphatic-venule tethering and network structure. The ability of venomotion to mechanically modulate lymph flow in the bat wing would be influenced by three structural properties. First, the degree of mechanical coupling depends on properties of the tissue tethering one side of the lymphangion to the venule and the other side of the lymphangion to the adjacent interstitial matrix. If the intervascular tissue stiffness were too low, venomotion would not displace one wall of the lymphangion. Similarly, the tissue tethering the other wall of the lymphangion to the adjacent interstitial matrix must be sufficiently stiff to hold it in place, otherwise venomotion would merely displace the entire lymphatic vessel without compressing or expanding it.

Second, to ensure that venular and lymphangion contraction can remain coordinated throughout the network, the depolarization waves along venules and lymphatic microvessels must travel with similar velocities, or else venular and lymphatic contractions would eventually become discoordinated. Alternatively, there could be electrical discontinuities allowing resynchronization by mechanical triggering. Third, it would be expected that lymphangions would lie in close proximity only to venules that have significant venomotion. In fact, lymphatic microvessels do not lie adjacent to parallel venules with diameters <25 μm where the lack of smooth muscle precludes spontaneous venomotion (148). Furthermore, lymphatic microvessels tend to switch sides and lie adjacent to parallel arterioles where venomotion is diminished.

Implications of interaction between extrinsic and intrinsic pumping of lymph. Although the rather pronounced venomotion of the bat wing may be unique (148), the coupling of intrinsic and extrinsic pumping may not be. Unlike common animal models, the bat wing model does not require anesthesia, which is known to decrease the magnitude of venomotion (26). Significant venomotion has not only been directly observed only in the bat wing, but has been inferred from venous pressure measurements in rabbit ear and dog limbs (72, 156, 157). Noddeland et al. (117) recorded rhythmic pressure oscillations in cannulated small veins of human feet and suggested that these oscillations were of venular origin. Recent recordings of the blood flow velocity in human feet by Lurie et al. (100, 101) exhibit rhythmic patterns similar to bat wing venular blood flow, suggesting a venular origin of the oscillations. Perhaps venomotion in the normal, resting state in other mammals is great enough to produce venomotion-

enhanced propulsion of lymph. Even if this is not the case, the present work suggests that other manifestations of extrinsic pumping, such as that arising from contraction of skeletal muscle, might also trigger, coordinate, and enhance intrinsic lymphangion pumping.

REFERENCES

1. **Allen SJ, Drake RE, Katz J, Gabel JC, Laine GA**. Lowered pulmonary arterial pressure prevents edema after endotoxin in sheep. *J Appl Physiol* 63: 1008-1011, 1987.
2. **Almen T, Standertskjold N**. Effects of dyes on microvasculature of the bat wing in vivo. *Invest Radiol* 4: 63-67, 1969.
3. **Amelang E, Prasad CM, Raymond RM, Grega GJ**. Interactions among inflammatory mediators on edema formation in the canine forelimb. *Circ Res* 49: 298-306, 1981.
4. **Arturson G, Mellander S**. Acute changes in capillary filtration and diffusion in experimental burn injury. *Acta Physiol Scand* 62: 457-463, 1964.
5. **Aukland K**. Distribution of body fluids: local mechanisms guarding interstitial fluid volume. *J Physiol* 79: 395-400, 1984.
6. **Aukland K, Reed RK**. Interstitial-lymphatic mechanisms in the control of extracellular fluid volume. *Physiol Rev* 73: 1-78, 1993.
7. **Benoit JN, Zawieja DC, Goodman AH, Granger HJ**. Characterization of intact mesenteric lymphatic pump and its responsiveness to acute edemagenic stress. *Am J Physiol Heart Circ Physiol* 257: H2059-H2069, 1989.
8. **Bentzer P, Kongstad L, Grande PO**. Capillary filtration coefficient is independent of number of perfused capillaries in cat skeletal muscle. *Am J Physiol Heart Circ Physiol* 280: H2697-H2706, 2001.

9. **Berg A, Ekwall AK, Rubin K, Stjernschantz J, Reed RK**. Effect of PGE1, PGI2, and PGF2 alpha analogs on collagen gel compaction in vitro and interstitial pressure in vivo. *Am J Physiol Heart Circ Physiol* 274: H663-H671, 1998.

10. **Berg A, Rubin K, Reed RK**. Cytochalasin D induces edema formation and lowering of interstitial fluid pressure in rat dermis. *Am J Physiol Heart Circ Physiol* 281: H7-H13, 2001.

11. **Bernard GR, Snapper JR, Hutchison AA, Brigham KL**. Effects of left atrial pressure elevation and histamine infusion on lung lymph in awake sheep. *J Appl Physiol* 56: 1083-1089, 1984.

12. **Bert JL, Bowen BD, Reed RK**. Microvascular exchange and interstitial volume regulation in the rat: model validation. *Am J Physiol Heart Circ Physiol* 254: H384-H399, 1988.

13. **Bert JL, Gyenge CC, Bowen BD, Reed RK, Lund T**. A model of fluid and solute exchange in the human: validation and implications. *Acta Physiol Scand* 170: 201-209, 2000.

14. **Blankfield RP, Finkelhor RS, Alexander JJ, Flocke SA, Maiocco J, Goodwin M, Zyzanski SJ**. Etiology and diagnosis of bilateral leg edema in primary care. *The Am J Med* 105: 192-197, 1998.

15. **Bouskela E**. Vasomotion frequency and amplitude related to intraluminal pressure and temperature in the wing of the intact, unanesthetized bat. *Microvasc Res* 37: 339-351, 1989.

16. **Bouskela E, Wiederhielm CA**. Microvascular myogenic reaction in the wing of the intact unanesthetized bat. *Am J Physiol Heart Circ Physiol* 237: H59-H65, 1979.

17. **Brennan MJ, Miller LT**. Overview of treatment options and review of the current role and use of compression garments, intermittent pumps, and exercise in the management of lymphedema. *Cancer* 83: 2821-2827, 1998.

18. **Bresler EH, Groome LJ**. On equations for combined convective and diffusive transport of neutral solute across porous membranes. *Am J Physiol Renal Physiol* 241: F469-F476, 1981.

19. **Brigham KL, Owen PJ**. Increased sheep lung vascular permeability caused by histamine. *Cir Res* 37: 647-657, 1975.

20. **Casley-Smith JR**. Mechanisms in the formation of lymph. *Int Rev Physiol* 26: 147-187, 1982.

21. **Casley-Smith JR**. The role of the endothelial intercellular junctions in the functioning of the initial lymphatics. *Angiologica* 9: 106-131, 1972.

22. **Chapple C, Bowen BD, Reed RK, Xie SL, Bert JL**. A model of human microvascular exchange: parameter estimation based on normals and nephrotics. *Comput Methods Programs Biomed* 41: 33-54, 1993.

23. **Cheville AL, McGarvey CL, Petrek JA, Russo SA, Taylor ME, Thiadens SR**. Lymphedema management. *Semin Radiat Oncol* 13: 290-301, 2003.

24. **Cho S, Atwood JE**. Peripheral edema. *Am J Med* 113: 580-586, 2002.

25. **Cliff WJ, Nicoll PA**. Structure and function of lymphatic vessels of the bat's wing. *Q J Exp Physiol Cogn Med Sci* 55: 112-131, 1970.

26. **Colantuoni A, Bertuglia S, Intaglietta M**. Effects of anesthesia on the spontaneous activity of the microvasculature. *Int J Microcirc Clin Exp* 3: 13-28, 1984.

27. **Davis MJ**. Microvascular control of capillary pressure during increases in local arterial and venous pressure. *Am J Physiol Heart Circ Physiol* 254: H772-H784, 1988.

28. **Davis MJ**. Control of bat wing capillary pressure and blood flow during reduced perfusion pressure. *Am J Physiol Heart Circ Physiol* 255: H1114-H1129, 1988.

29. **Davis MJ**. Spontaneous contractions of isolated bat wing venules are inhibited by luminal flow. *Am J Physiol Heart Circ Physiol* 264: H1174-H1186, 1993.

30. **Davis MJ, Shi X, Sikes PJ**. Modulation of bat wing venule contraction by transmural pressure changes. *Am J Physiol Heart Circ Physiol* 262: H625-H634, 1992.

31. **Davis MJ, Sikes PJ**. A rate-sensitive component to the myogenic response is absent from bat wing arterioles. *Am J Physiol Heart Circ Physiol* 256: H32-H40, 1989.

32. **Davis MJ, Sikes PJ, Davis KL, Granger HJ, Zawieja DC**. Venular vasomotion enhances lymphatic pump function (Abstract). In: *Proc 31st Int Congr Physiol Sci*. Helsinki: pp. 375, 1989.

33. **Dobbins DE, Swindall BT, Haddy FJ, Dabney JM**. Blockade of histamine-mediated increases in microvascular permeability by H1- and H2-receptor antagonists. *Microvasc Res* 21: 343-350, 1981.

34. **Dongaonkar RM, Quick CM, Stewart RH, Drake RE, Cox CS, Jr., Laine GA**. Edemagenic gain and interstitial fluid volume regulation. *Am J Physiol Regul Integr Comp Physiol* 294: R651-R659, 2008.

35. **Drake R, Gaar KA, Taylor AE**. Estimation of the filtration coefficient of pulmonary exchange vessels. *Am J Physiol Heart Circ Physiol* 234: H266-H274, 1978.

36. **Drake R, Giesler M, Laine G, Gabel J, Hansen T**. Effect of outflow pressure on lung lymph flow in unanesthetized sheep. *J Appl Physiol* 58: 70-76, 1985.

37. **Drake RE, Adcock DK, Scott RL, Gabel JC**. Effect of outflow pressure upon lymph flow from dog lungs. *Circ Res* 50: 865-869, 1982.

38. **Drake RE, Allen SJ, Katz J, Gabel JC, Laine GA**. Equivalent circuit technique for lymph flow studies. *Am J Physiol Heart Circ Physiol* 251: H1090-H1094, 1986.

39. **Drake RE, Allen SJ, Williams JP, Laine GA, Gabel JC**. Lymph flow from edematous dog lungs. *J Appl Physiol* 62: 2416-2420, 1987.

40. **Drake RE, Laine GA**. Pulmonary microvascular permeability to fluid and macromolecules. *J Appl Physiol* 64: 487-501, 1988.

41. **Drake RE, Smith JH, Gabel JC**. Estimation of the filtration coefficient in intact dog lungs. *Am J Physiol Heart Circ Physiol* 238: H430-H438, 1980.

42. **Dunbar BS, Elk JR, Drake RE, Laine GA**. Intestinal lymphatic flow during portal venous hypertension. *Am J Physiol Gastrointest Liver Physiol* 257: G94-G98, 1989.

43. **Ehrhart IC, Granger WM, Hofman WF**. Filtration coefficient obtained by stepwise pressure elevation in isolated dog lung. *J Appl Physiol* 56: 862-867, 1984.

44. **Elk JR, Drake RE, Williams JP, Gabel JC, Laine GA**. Lymphatic function in the liver after hepatic venous pressure elevation. *Am J Physiol Gastrointest Liver Physiol* 254: G748-G752, 1988.

45. **Erdmann AJ, 3rd, Vaughan TR, Jr., Brigham KL, Woolverton WC, Staub NC**. Effect of increased vascular pressure on lung fluid balance in unanesthetized sheep. *Circ Res* 37: 271-284, 1975.

46. **Ferguson MK, Shahinian HK, Michelassi F**. Lymphatic smooth muscle responses to leukotrienes, histamine and platelet activating factor. *J Surg Res* 44: 172-177, 1988.

47. **Fox JL, von der Weid PY**. Effects of histamine on the contractile and electrical activity in isolated lymphatic vessels of the guinea-pig mesentery. *Br J Pharmacol* 136: 1210-1218, 2002.

48. **Franco de Carvalho E, Parra ER, de Souza R, Muxfeldt A'b Saber A, Capelozzi VL**. Parenchymal and vascular interactions in the pathogenesis of nonspecific interstitial pneumonia in systemic sclerosis and idiopathic interstitial pneumonia. *Respiration* 76: 146-153, 2008.

49. **Franklin GF, Powell JD, Emami-Naeini A**. *Feedback Control of Dynamic Systems*. Upper Saddle River, NJ: Prentice Hall, 2005.

50. **Fronek K, Zweifach BW**. Microvascular pressure distribution in skeletal muscle and the effect of vasodilation. *Am J Physiol* 228: 791-796, 1975.

51. **Fung YC**. *Biomechanics: Mechanical Properties of Living Tissues*. New York, NY: Springer-Verlag, 1993.

52. **Gaar KA, Jr., Taylor AE, Owens LJ, Guyton AC**. Pulmonary capillary pressure and filtration coefficient in the isolated perfused lung. *Am J Physiol* 213: 910-914, 1967.

53. **Gabel JC, Hansen TN, Drake RE**. Effect of endotoxin on lung fluid balance in unanesthetized sheep. *J Appl Physiol* 56: 489-494, 1984.

54. **Gashev AA, Davis MJ, Zawieja DC**. Inhibition of the active lymph pump by flow in rat mesenteric lymphatics and thoracic duct. *J Physiol* 540: 1023-1037, 2002.

55. **Gashev AA, Zawieja DC**. Physiology of human lymphatic contractility: a historical perspective. *Lymphology* 34: 124-134, 2001.

56. **Gibbons GH, Dzau VJ**. The emerging concept of vascular remodeling. *N Engl J Med* 330: 1431-1438, 1994.

57. **Gjerde EA, Woie K, Wei ET, Reed RK**. Lowering of interstitial fluid pressure after neurogenic inflammation is inhibited by mystixin-7 peptide. *Am J Physiol Heart Circ Physiol* 279: H1377-H1382, 2000.

58. **Goldberg HS**. Pulmonary interstitial compliance and microvascular filtration coefficient. *Am J Physiol Heart Circ Physiol* 239: H189-H198, 1980.

59. **Gore RW, Bohlen HG**. Pressure regulation in the microcirculation. *Fed Proc* 34: 2031-2037, 1975.

60. **Granger DN, Taylor AE**. Permeability of intestinal capillaries to endogenous macromolecules. *Am J Physiol Heart Circ Physiol* 238: H457-H464, 1980.

61. **Greenway CV, Lautt WW**. Effects of hepatic venous pressure on transsinusoidal fluid transfer in the liver of the anesthetized cat. *Circ Res* 26: 697-703, 1970.

62. **Guyton AC**. Determination of cardiac output by equating venous return curves with cardiac response curves. *Physiol Rev* 35: 123-129, 1955.

63. **Guyton AC**. Interstitial fluid pressure. II. Pressure-volume curves of interstitial space. *Circ Res* 16: 452-460, 1965.

64. **Guyton AC**. Long-term arterial pressure control: an analysis from animal experiments and computer and graphic models. *Am J Physiol Regul Integr Comp Physiol* 259: R865-R877, 1990.

65. **Guyton AC, Coleman TG**. Regulation on interstitial fluid volume and pressure. *Ann N Y Acad Sci* 150: 537-547, 1968.

66. **Guyton AC, Granger HJ, Taylor AE**. Interstitial fluid pressure. *Physiol Rev* 51: 527-563, 1971.

67. **Guyton AC, Hall JE**. *Textbook of Medical Physiology*. Philadelphia: WB Saunders Company, 2000.

68. **Guyton AC, Lindsey AW**. Effect of elevated left atrial pressure and decreased plasma protein concentration on the development of pulmonary edema. *Circ Res* 7: 649-657, 1959.

69. **Guyton AC, Taylor AE, Brace RA**. A synthesis of interstitial fluid regulation and lymph formation. *Fed Proc* 35: 1881-1885, 1976.

70. **Gyenge CC, Bowen BD, Reed RK, Bert JL**. Transport of fluid and solutes in the body I. Formulation of a mathematical model. *Am J Physiol Heart Circ Physiol* 277: H1215-H1227, 1999.

71. **Gyenge CC, Bowen BD, Reed RK, Bert JL**. Transport of fluid and solutes in the body II. Model validation and implications. *Am J Physiol Heart Circ Physiol* 277: H1228-H1240, 1999.

72. **Haddy FJ, Richards AG, Alden JL, Visscher MB**. Small vein and artery pressures in normal and edematous extremities of dogs under local and general anesthesia. *Am J Physiol* 176: 355-360, 1954.

73. **Haddy FJ, Scott JB, Grega GJ**. Effects of histamine on lymph protein concentration and flow in the dog forelimb. *Am J Physiol* 223: 1172-1177, 1972.

74. **Hara N, Nagashima A, Yoshida T, Furukawa T, Inokuchi K**. Effect of decreased plasma colloid osmotic pressure on development of pulmonary edema in dogs. *Jpn J Surg* 11: 203-208, 1981.

75. **Hargens AR, Zweifach BW**. Contractile stimuli in collecting lymph vessels. *Am J Physiol Heart Circ Physiol* 233: H57-H65, 1977.

76. **Hashimoto S, Kawai Y, Ohhashi T**. Effects of vasoactive substances on the pig isolated hepatic lymph vessels. *J Pharmacol Exp Ther* 269: 482-488, 1994.

77. **Hattori J, Yamakage M, Seki S, Okazaki K, Namiki A**. Inhibitory effects of the anesthetics propofol and sevoflurane on spontaneous lymphatic vessel activity in rats. *Anesthesiology* 101: 687-694, 2004.

78. **Johnson PC**. Effect of venous pressure on mean capillary pressure and vascular resistance in the intestine. *Circ Res* 16: 294-300, 1965.

79. **Johnson PC, Hanson KM**. Capillary filtration in the small intestine of the dog. *Circ Res* 19: 766-773, 1966.

80. **Johnson PC, Richardson DR**. The influence of venous pressure on filtration forces in the intestine. *Microvasc Res* 7: 296-306, 1974.

81. **Jones TW**. Discovery that the veins of the bat's wing (which are furnished with valves) are endowed with rythmical contractility, and that the onward flow of blood is accelerated by each contraction. *Phil Trans R Soc Lond* 142: 131-136, 1852.

82. **Kallen FC**. The active venous pulse in the wing circulation of bats (Chiroptera). Overview of circulation in the wing membrane. *Experientia* 34: 1398-1400, 1978.

83. **Karlsen TV, Bletsa A, Gjerde EA, Reed RK**. Lowering of interstitial fluid pressure after neurogenic inflammation in mouse skin is partly dependent on mast cells. *Am J Physiol Heart Circ Physiol* 292: H1821-H1827, 2007.

84. **Kedem O, Katchalsky A**. Thermodynamic analysis of the permeability of biological membranes to non-electrolytes. *Biochim Biophys Acta* 27: 229-246, 1958.

85. **Kluger MJ, Heath JE**. Vasomotion in the bat wing: a thermoregulatory response to internal heating. *Comp Biochem Physiol* 32: 219-226, 1970.

86. **Koller ME, Reed RK**. Increased negativity of interstitial fluid pressure in rat trachea in dextran anaphylaxis. *J Appl Physiol* 72: 53-57, 1992.

87. **Koller ME, Woie K, Reed RK**. Increased negativity of interstitial fluid pressure in rat trachea after mast cell degranulation. *J Appl Physiol* 74: 2135-2139, 1993.

88. **Korthuis RJ, Wang CY, Spielman WS**. Transient effects of histamine on the capillary filtration coefficient. *Microvasc Res* 28: 322-344, 1984.

89. **Kuo BC, Golnaraghi F**. *Automatic Control Systems*. New York: Wiley, 2002.

90. **Laine GA, Allen SJ, Katz J, Gabel JC, Drake RE**. Effect of systemic venous pressure elevation on lymph flow and lung edema formation. *J Appl Physiol* 61: 1634-1638, 1986.

91. **Laine GA, Allen SJ, Katz J, Gabel JC, Drake RE**. Outflow pressure reduces lymph flow rate from various tissues. *Microvasc Res* 33: 135-142, 1987.

92. **Laine GA, Allen SJ, Williams JP, Katz J, Gabel JC, Drake RE**. A new look at pulmonary edema. *News Physiol Sci*, 1: 150-153, 1986.

93. **Laine GA, Drake RE, Zavisca FG, Gabel JC**. Effect of lymphatic cannula outflow height on lung microvascular permeability estimations. *J Appl Physiol* 57: 1412-1416, 1984.

94. **Laine GA, Hall JT, Laine SH, Granger J**. Transsinusoidal fluid dynamics in canine liver during venous hypertension. *Circ Res* 45: 317-323, 1979.

95. **Landis EM**. Micro-injection studies of capillary permeability: II. The relation between capillary pressure and the rate at which fluid passes through the walls of single capillaries. *Am J Physiol* 82: 217-238, 1927.

96. **Leak LV, Schannahan A, Scully H, Daggett WM**. Lymphatic vessels of the mammalian heart. *Anat Rec* 191: 183-201, 1978.

97. **Levick JR**. Capillary filtration-absorption balance reconsidered in light of dynamic extravascular factors. *Exp Physiol* 76: 825-857, 1991.

98. **Levine OR, Mellins RB, Senior RM, Fishman AP**. The application of Starling's law of capillary exchange to the lungs. *J Clin Invest* 46: 934-944, 1967.

99. **Lund T, Onarheim H, Wiig H, Reed RK**. Mechanisms behind increased dermal imbibition pressure in acute burn edema. *Am J Physiol Heart Circ Physiol* 256: H940-H948, 1989.

100. **Lurie F, Kistner RL, Eklof B**. The mechanism of venous valve closure in normal physiologic conditions. *J Vasc Surg* 35: 713-717, 2002.

101. **Lurie F, Kistner RL, Eklof B, Kessler D**. Mechanism of venous valve closure and role of the valve in circulation: a new concept. *J Vasc Surg* 38: 955-961, 2003.

102. **Magno M, Atkinson B, Katz A, Fishman AP**. Estimation of pulmonary interstitial fluid space compliance in isolated perfused rabbit lung. *J Appl Physiol* 48: 677-683, 1980.

103. **Manning GS, Breseler EH, Wendt RP**. Irreversible thermodynamics and flow across membranes. *Science* 166: 1438, 1969.

104. **Marten K, Dicken V, Kneitz C, Hohmann M, Kenn W, Hahn D, Engelke C**. Interstitial lung disease associated with collagen vascular disorders: disease quantification using a computer-aided diagnosis tool. *Eur Radiol* 2008.

105. **McGeown JG, McHale NG, Thornbury KD**. The role of external compression and movement in lymph propulsion in the sheep hind limb. *J Physiol* 387: 83-93, 1987.

106. **McHale NG, Roddie IC**. The effect of transmural pressure on pumping activity in isolated bovine lymphatic vessels. *J Physiol* 261: 255-269, 1976.

107. **McHale NG, Thornbury KD**. The effect of anesthetics on lymphatic contractility. *Microvasc Res* 37: 70-76, 1989.

108. **McNamee JE**. Histamine decreases selectivity of sheep lung blood-lymph barrier. *J Appl Physiol* 54: 914-918, 1983.

109. **Michel CC**. Fluid movements through capillary walls. In: *Handbook of Physiology: The Cardiovascular System Microcircultion*. Bethesda, MD: Am. Physiol. Soc., sect. 2, Vol. IV, part 1, pp. 375-409, 1984.

110. **Michel CC, Curry FE**. Microvascular permeability. *Physiol Rev* 79: 703-761, 1999.

111. **Michel CC, Kendall S**. Differing effects of histamine and serotonin on microvascular permeability in anaesthetized rats. *J Physiol* 501: 657-662, 1997.

112. **Miserocchi G, Negrini D, Del Fabbro M, Venturoli D**. Pulmonary interstitial pressure in intact in situ lung: transition to interstitial edema. *J Appl Physiol* 74: 1171-1177, 1993.

113. **Miserocchi G, Negrini D, Gonano C**. Direct measurement of interstitial pulmonary pressure in in situ lung with intact pleural space. *J Appl Physiol* 69: 2168-2174, 1990.

114. **Mitzner W, Robotham JL**. Distribution of interstitial compliance and filtration coefficient in canine lung. *Lymphology* 12: 140-148, 1979.

115. **Nakahara K, Ohkuda K, Staub NC**. Effect of infusing histamine into pulmonary or bronchial artery on sheep pulmonary fluid balance. *Am Rev Respir Dis* 120: 875-882, 1979.

116. **Nakayama K, Tanaka Y**. Stretch-induced contraction and Ca2+ mobilization in vascular smooth muscle. *Biol Signals* 2: 241-252, 1993.

117. **Noddeland H, Nicolaysen G, Aukland K**. Rhythmic variations of venous pressure in the human foot. *Acta Physiol Scand* 113: 125-127, 1981.

118. **Oliver G**. Lymphatic vasculature development. *Nat Rev Immunol* 4: 35-45, 2004.

119. **Ostgaard G, Reed RK**. Increased negatively of interstitial fluid pressure in rat skin contributes to the edema formation induced by Zymosan. *Microvasc Res* 46: 283-292, 1993.

120. **Pappenheimer JR, Soto-Rivera A**. Effective osmotic pressure of the plasma proteins and other quantities associated with the capillary circulation in the hindlimbs of cats and dogs. *Am J Physiol* 152: 471-491, 1948.

121. **Parker JC, Guyton AC, Taylor AE**. Pulmonary interstitial and capillary pressures estimated from intra-alveolar fluid pressures. *J Appl Physiol* 44: 267-276, 1978.

122. **Parker JC, Perry MA, Taylor AE**. Permeability of the microvascular barrier. In: *Edema*, edited by Staub NC, and Taylor AE. New York: Raven, pp. 143-187, 1984.

123. **Patlak CS, Goldstein DA, Hoffman JF**. The flow of solute and solvent across a two-membrane system. *J Theor Biol* 5: 426-442, 1963.

124. **Pietra GG, Szidon JP, Leventhal MM, Fishman AP**. Histamine and interstitial pulmonary edema in the dog. *Circ Res* 29: 323-337, 1971.

125. **Powell AA, Armstrong MA**. Peripheral edema. *Am Fam Physician* 55: 1721-1726, 1997.

126. **Quick CM, Venugopal AM, Dongaonkar RM, Laine GA, Stewart RH**. First-order approximation for the pressure-flow relationship of spontaneously contracting lymphangions. *Am J Physiol Heart Circ Physiol* 294: H2144-H2149, 2008.

127. **Reddy NP, Staub NC**. Intrinsic propulsive activity of thoracic duct perfused in anesthetized dogs. *Microvasc Res* 21: 183-192, 1981.

128. **Reed RK, Berg A, Gjerde EA, Rubin K**. Control of interstitial fluid pressure: role of beta1-integrins. *Semin Nephrol* 21: 222-230, 2001.

129. **Reed RK, Bowen BD, Bert JL**. Microvascular exchange and interstitial volume regulation in the rat: implications of the model. *Am J Physiol Heart Circ Physiol* 257: H2081-H2091, 1989.

130. **Reed RK, Rodt SA**. Increased negativity of interstitial fluid pressure during the onset stage of inflammatory edema in rat skin. *Am J Physiol Heart Circ Physiol* 260: H1985-H1991, 1991.

131. **Reed RK, Wiig H**. Compliance of the interstitial space in rats. I. Studies on hindlimb skeletal muscle. *Acta Physiol Scand* 113: 297-305, 1981.

132. **Reed RK, Woie K, Rubin K**. Integrins and control of interstitial fluid pressure. *News Physiol Sci* 12: 42-49, 1997.

133. **Reeder LB, DeFilippi VJ, Ferguson MK**. Characterization of the effects of histamine in porcine tracheobronchial lymph vessels. *Am J Physiol Heart Circ Physiol* 271: H2501-H2507, 1996.

134. **Rodt SA, Wiig H, Reed RK**. Increased negativity of interstitial fluid pressure contributes to development of oedema in rat skin following application of xylene. *Acta Physiol Scand* 140: 581-586, 1990.

135. **Schmid-Schonbein GW**. Mechanisms causing initial lymphatics to expand and compress to promote lymph flow. *Arch Histol Cytol* 53 Suppl: 107-114, 1990.

136. **Schmid-Schonbein GW**. Microlymphatics and lymph flow. *Physiol Rev* 70: 987-1028, 1990.

137. **Skalak TC, Schmid-Schonbein GW, Zweifach BW**. New morphological evidence for a mechanism of lymph formation in skeletal muscle. *Microvasc Res* 28: 95-112, 1984.

138. **Srinivasan RS, Dillard ME, Lagutin OV, Lin FJ, Tsai S, Tsai MJ, Samokhvalov IM, Oliver G**. Lineage tracing demonstrates the venous origin of the mammalian lymphatic vasculature. *Genes Dev* 21: 2422-2432, 2007.

139. **Starling EH**. On the absorption of fluids from the connective tissue spaces. *J Physiol* 19: 312-326, 1896.

140. **Staub NC.** Pulmonary edema. *Physiol Rev* 54: 678-811, 1974.

141. **Stenmark KR, Davie N, Frid M, Gerasimovskaya E, Das M**. Role of the adventitia in pulmonary vascular remodeling. *Physiology* 21: 134-145, 2006.

142. **Stewart RH, Geissler HJ, Allen SJ, Laine GA**. Protein washdown as a defense mechanism against myocardial edema. *Am J Physiol Heart Circ Physiol* 279: H1864-H1868, 2000.

143. **Stewart RH, Laine GA**. Flow in lymphatic networks: interaction between hepatic and intestinal lymph vessels. *Microcirc* 8: 221-227, 2001.

144. **Swartz MA**. The physiology of the lymphatic system. *Adv Drug Deliv Rev* 50: 3-20, 2001.

145. **Swartz MA, Boardman KC, Jr.** The role of interstitial stress in lymphatic function and lymphangiogenesis. *Ann N Y Acad Sci* 979: 197-210; discussion 229-134, 2002.

146. **Takahashi N, Kawai Y, Ohhashi T**. Effects of vasoconstrictive and vasodilative agents on lymphatic smooth muscles in isolated canine thoracic ducts. *J Pharmacol Exp Ther* 254: 165-170, 1990.

147. **Taylor AE, Granger DN**. Exchange of macromolecules across the microcirculation. In: *Handbook of Physiology: The Cardiovascular System Microcircultion*. Bethesda, MD: Am. Physiol. Soc., sect. 2, Vol. IV, part 1, pp. 465-520, 1984.

148. **Torres Filho IP**. Venular vasomotion in the bat wing. *Microvasc Res* 39: 246-249, 1990.

149. **Wangensteen OD, Lysaker E, Savaryn P**. Pulmonary capillary filtration and reflection coefficients in the adult rabbit. *Microvasc Res* 14: 81-97, 1977.

150. **Webb RL, Nicoll PA**. Behavior of lymphatic vessels in the living bat. A*nat Rec* 88: 351-367, 1944.

151. **Webster HL**. Colloid osmotic pressure: theoretical aspects and background. *Clin Perinatol* 9: 505-521, 1982.

152. **Widmer RJ, Laurinec JE, Young MF, Laine GA, Quick CM**. Local heat produces a shear-mediated biphasic response in the thermoregulatory microcirculation of the Pallid bat wing. *Am J Physiol Regul Integr Comp Physiol* 291: R625-R632, 2006.

153. **Widmer RJ, Stewart RH, Young MF, Laurinec JE, Laine GA, Quick CM**. Application of local heat induces capillary recruitment in the Pallid bat wing. *Am J Physiol Regul Integr Comp Physiol* 292: R2312-R2317, 2007.

154. **Wiedeman MP**. Effect of venous flow on frequency of venous vasomotion in the bat wing. *Circ Res* 5: 641-644, 1957.

155. **Wiedeman MP**. Pressure variations in small veins in the hindleg of the dog. *Circ Res* 8: 440-445, 1960.

156. **Wiedeman MP**. Preparation of the bat wing for in vivo microscopy. *Microvasc Res* 5: 417-422, 1973.

157. **Wiedeman MP**. Relevance of work on bats to our understanding of the role of active venous vasomotion in the circulatory system. *Experientia* 34: 1421, 1978.

158. **Wiederhielm CA**. Effects of temperature and transmural pressure on contractile activity of vascular smooth muscle. *Bibl Anat* 9: 321-327, 1967.

159. **Wiig H**. Comparison of methods for measurement of interstitial fluid pressure in cat skin/subcutis and muscle. *Am J Physiol Heart Circ Physiol* 249: H929-H944, 1985.

160. **Wiig H, Reed RK**. Volume-pressure relationship (compliance) of interstitium in dog skin and muscle. *Am J Physiol Heart Circ Physiol* 253: H291-H298, 1987.

161. **Wiig H, Reed RK, Aukland K**. Measurement of interstitial fluid pressure in dogs: evaluation of methods. *Am J Physiol Heart Circ Physiol* 253: H283-H290, 1987.

162. **Wiig H, Reed RK, Aukland K**. Measurement of interstitial fluid pressure: comparison of methods. *Ann Biomed Eng* 14: 139-151, 1986.

163. **Wiig H, Rubin K, Reed RK**. New and active role of the interstitium in control of interstitial fluid pressure: potential therapeutic consequences. *Acta Anaesthesiol Scand* 47: 111-121, 2003.

164. **Woie K, Koller ME, Heyeraas KJ, Reed RK**. Neurogenic inflammation in rat trachea is accompanied by increased negativity of interstitial fluid pressure. *Circ Res* 73: 839-845, 1993.

165. **Woie K, Ree RK**. The relationship between interstitial fluid pressure and volume in rat trachea. *Acta Physiol Scand* 156: 69-74, 1996.

166. **Xie SL, Reed RK, Bowen BD, Bert JL**. A model of human microvascular exchange. *Microvasc Res* 49: 141-162, 1995.

167. **Zawieja D**. Lymphatic biology and the microcirculation: past, present and future. *Microcirc* 12: 141-150, 2005.

168. **Zoltzer H**. Initial lymphatics--morphology and function of the endothelial cells. *Lymphology* 36: 7-25, 2003.

APPENDIX A

A

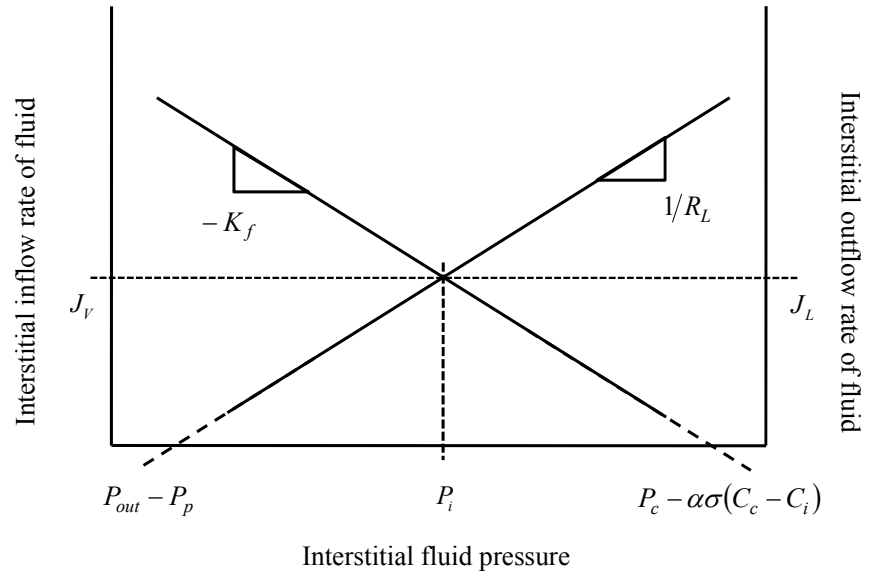

B

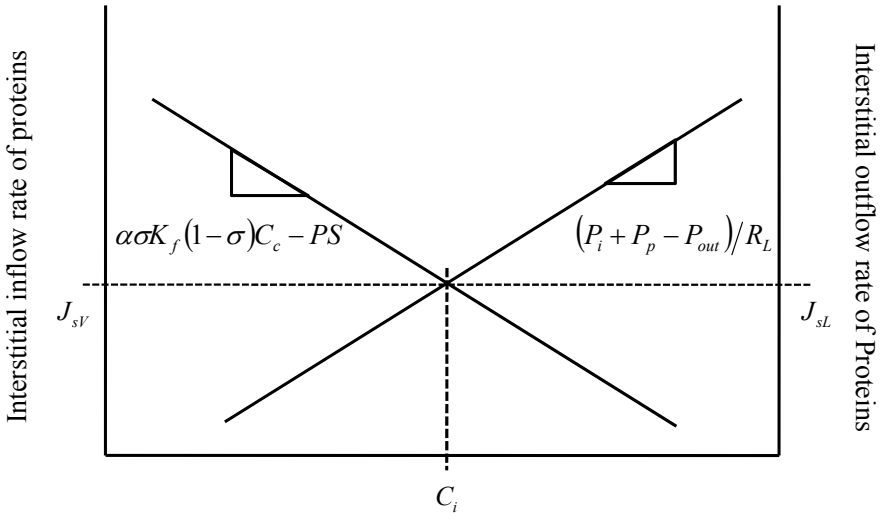

Figure A-1. Graphical representation of the balance point concept applied to interstitial fluid and protein flow. A) Graphical representation of the relationship between P_i and J_V (*Eq. 3.2*) and P_i and J_L (*Eq. 3.4*). Their slopes are equal to $-K_f$ and $1/R_L$, respectively. Steady-state values of P_i, J_L and J_V are represented by the intersection. B) Graphical representation of the relationship between C_i and J_{sV} (*Eq. 3.3*) and C_i and J_{sL}. (*Eq. 3.5*). Their slopes are equal to $\alpha\sigma K_f(1-\sigma)C_c - PS$ and $(P_i+P_p-P_{out})/R_L$, respectively. Steady-state values of C_i, J_{sV} and J_{sL} are represented by the intersection.

A

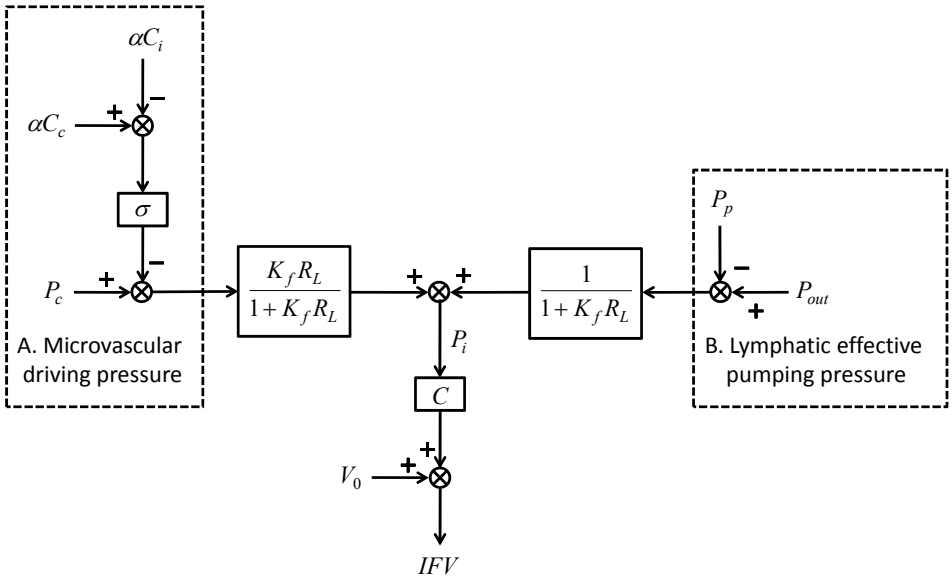

B

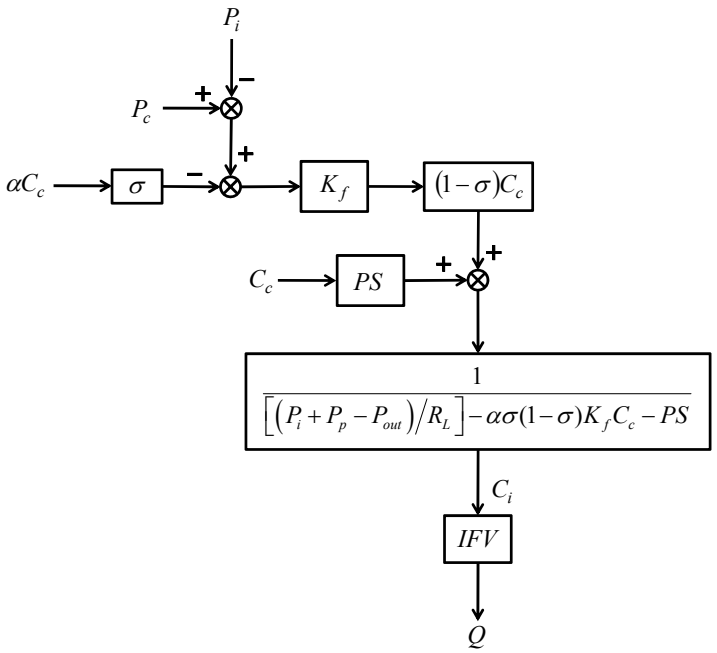

Figure A-2. A) Block diagram of interstitial fluid volume regulation at steady-state constructed from *Eqs. 3.2, 3.4* and *3.6a*. The microvascular filtration coefficient (K_f) and the effective lymphatic resistance (R_L) determine interstitial fluid pressure (P_i) by modulating microvascular driving pressure (part I) and lymphatic effective pumping pressure (part II). P_i is not affected by interstitial compliance (C). B) Block diagram of interstitial protein regulation at steady-state constructed from *Eqs. 3.3, 3.5* and *3.6b*. Structural parameters (K_f, σ, and PS) along with lymphatic outflow rate (J_L) determine interstitial protein concentration (C_i).

A

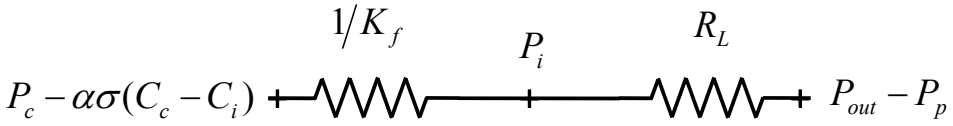

$$P_i = \frac{R_L}{1/K_f + R_L}\left[P_c - \alpha\sigma\left(C_c - C_i\right)\right] + \frac{1/K_f}{1/K_f + R_L}\left(P_{out} - P_p\right)$$

B

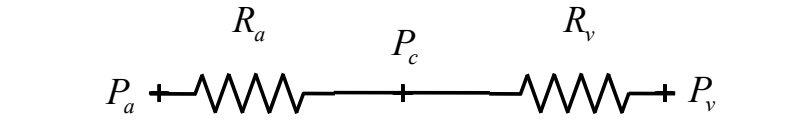

$$P_c = \frac{R_v}{R_a + R_v}P_a + \frac{R_a}{R_a + R_v}P_v$$

Figure A-3. Steady-state interstitial fluid pressure regulation is analogous to microvascular pressure regulation. A) Representation of steady-state interstitial fluid pressure balance point in terms of inflow and outflow resistances. B) Representation of steady-state capillary pressure regulation in terms of arterial and venular resistances. $1/K_f$ and R_L are analogous to arteriolar resistance (R_a) and venular resistance (R_v). The ratio of interstitial inflow resistance ($1/K_f$) and interstitial outflow resistance (R_L) determines whether P_i approaches microvascular driving pressure [P_c-$\alpha\sigma$(C_c-C_i)] or lymphatic effective pumping pressure (P_{out}-P_p).

A

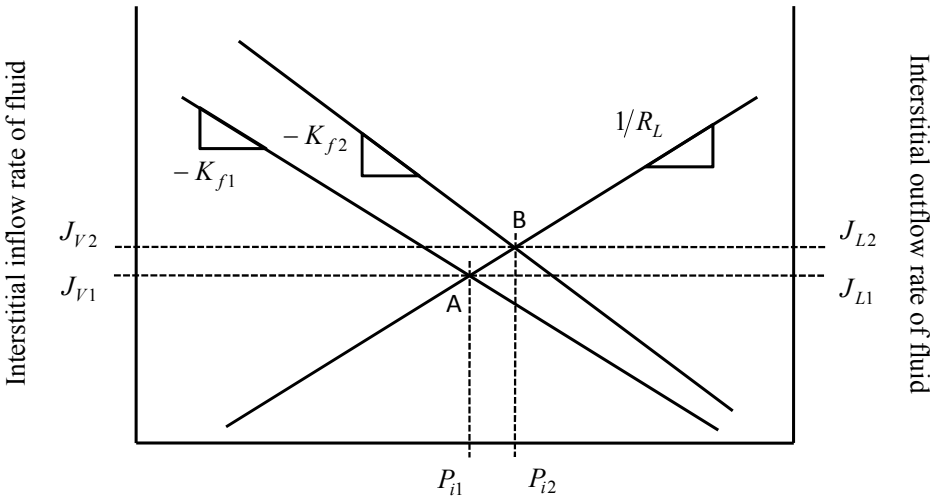

B

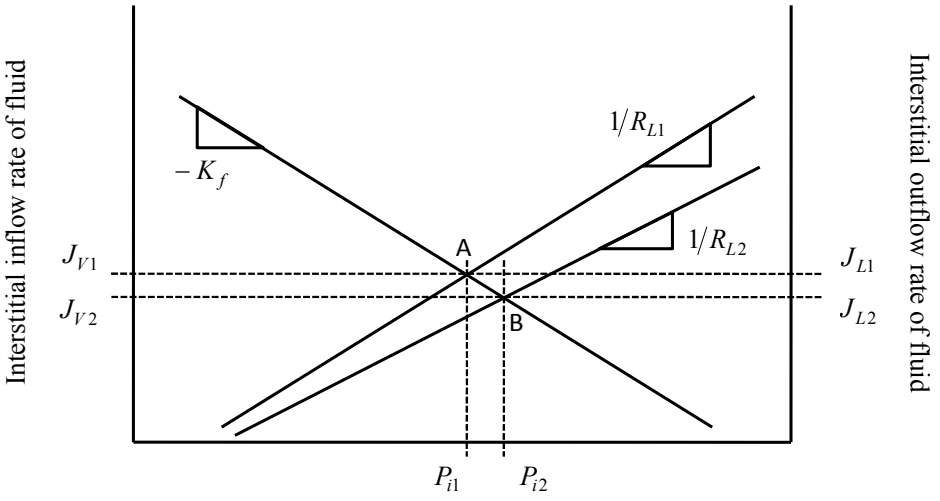

Figure A-4. Graphical balance point analysis illustrated in Fig. A-2 provides intuitive insight into interstitial fluid pressure regulation. Effect of changing various parameters and variables on interstitial fluid pressure (P_i), microvascular fluid filtration (J_v) and lymph outflow of fluid (J_L) illustrated by a shift in the balance point from A to B. Subscripts indicate change from *state 1* to *state 2*. Effect of increasing microvascular filtration coefficient K_f (A), increasing effective lymphatic resistance R_L (B), increasing capillary pressure P_c (C), increasing lymphatic outlet pressure P_{out} (D), concomitant increase in K_f and R_L increases interstitial fluid pressure, but maintains J_V and J_L (E), simultaneous increase in K_f and decrease R_L increases J_V and J_L, but maintains interstitial fluid pressure (F).

C

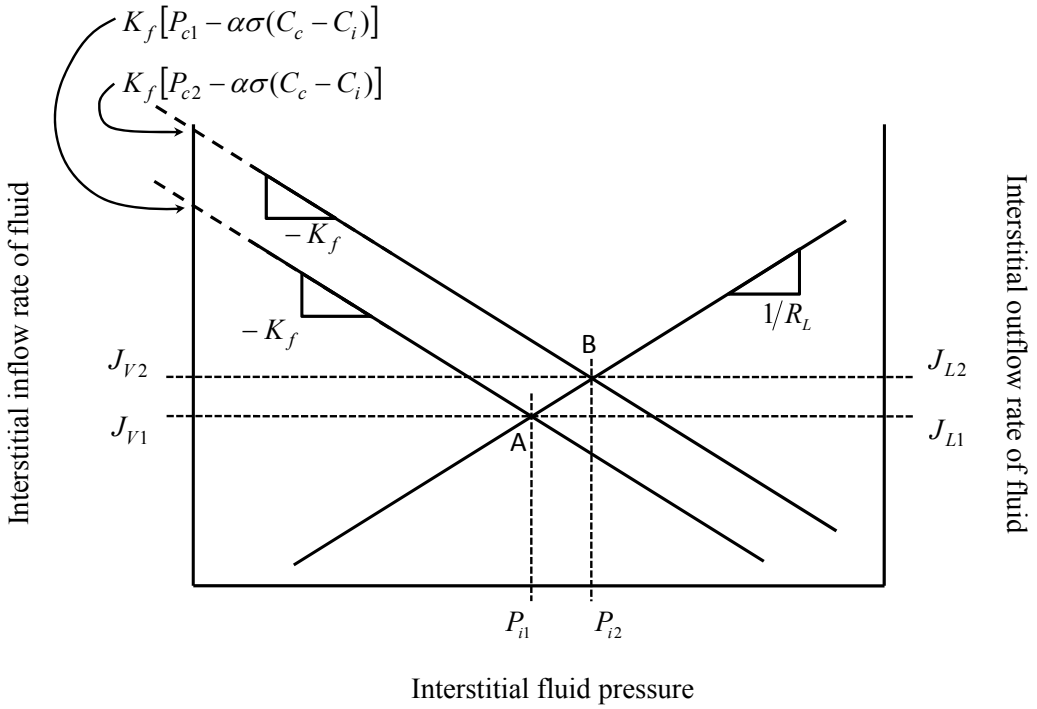

D

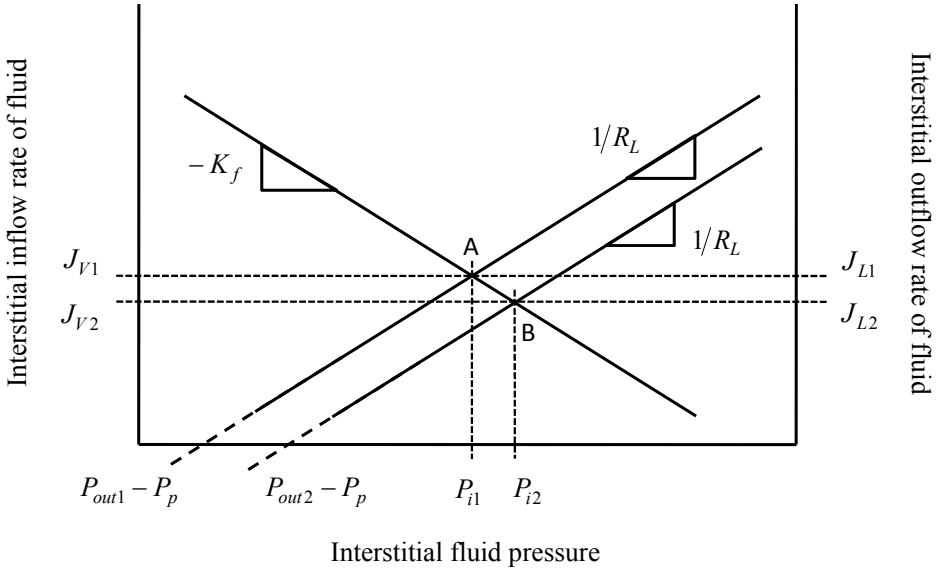

Figure A-4 continued.

E

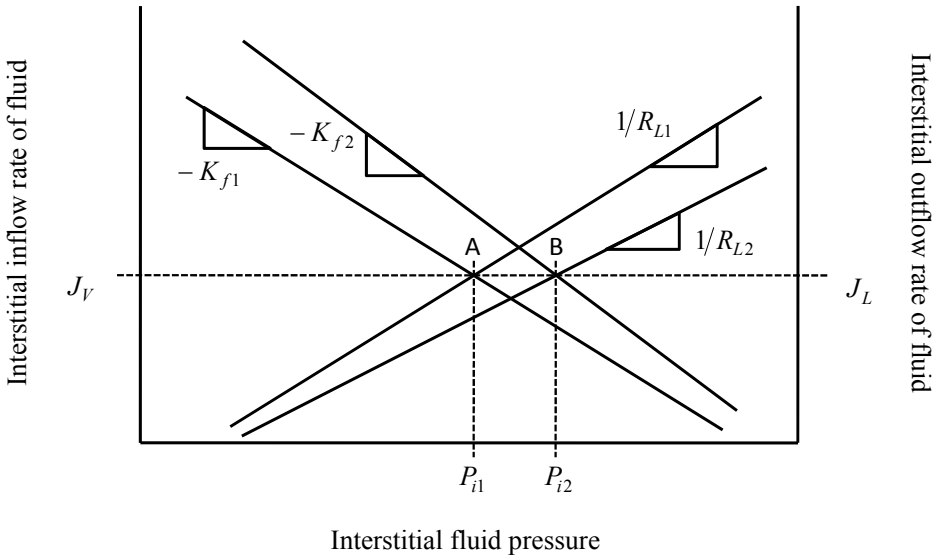

F

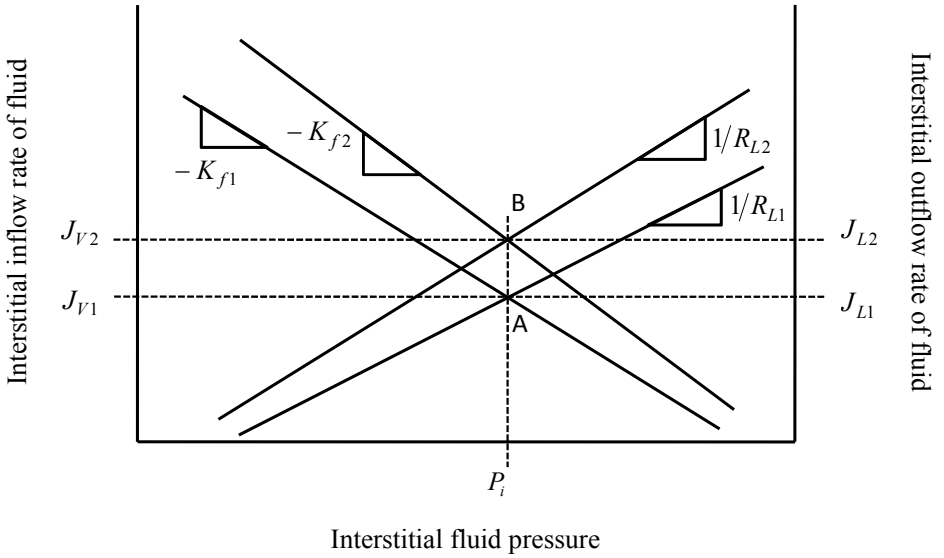

Figure A-4 continued.

A

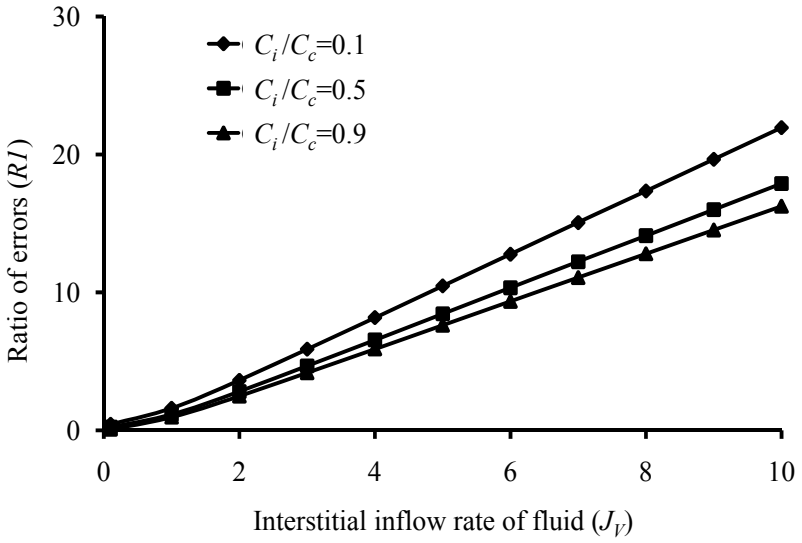

B

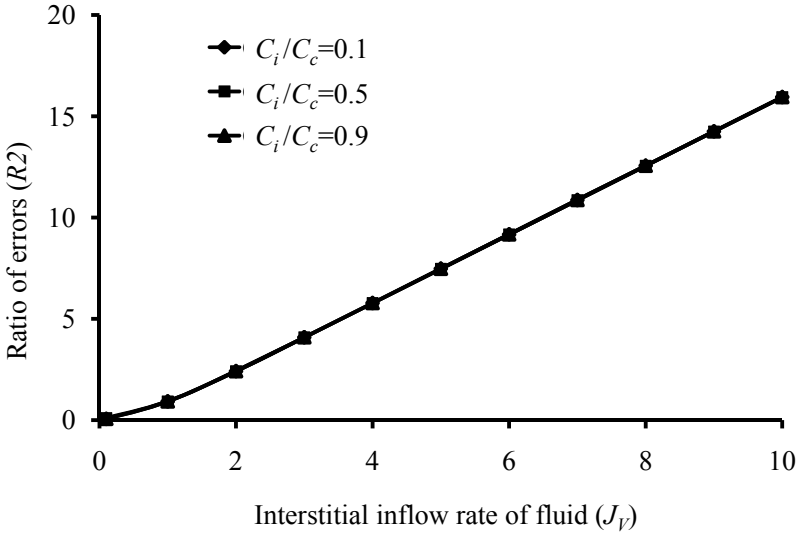

Figure A-5. Microvascular protein extravasation rate (J_{sV}) estimation using the Taylor-Granger formulation (J_{sV}^{TG}) (*Eq. 3.3*) is compared with the Kedem-Katchalsky formulation (J_{sV}^{KK}) (*Eq. C1*) and the Manning formulation (J_{sV}^{M}) (*Eq. C3*) assuming the Patlak-Hoffman formulation (J_{sV}^{PH}) (*Eq. C2*) is ideal (18). A) Ratio of errors $R1=|J_{sV}^{PH} - J_{sV}^{KK}|/|J_{sV}^{PH} - J_{sV}^{TG}|$ as a function of J_V compares the Taylor-Granger formulation with the Kedem-Katchalsky formulation assuming C_i/C_c = 0.1, 0.5 and 0.9 (σ = 0.6, PS = 0.118). B) Ratio of errors $R2=|J_{sV}^{PH} - J_{sV}^{M}|/|J_{sV}^{PH} - J_{sV}^{TG}|$ as a function of J_V compares the Taylor-Granger formulation with the Manning formulation assuming C_i/C_c = 0.1, 0.5 and 0.9 (σ = 0.6, PS = 0.118). The fact that $R1$ >1 and $R2$ >1 with increasing J_V suggests that the Taylor-Granger formulation is a better approximation of the Patlak-Hoffman formulation.

A

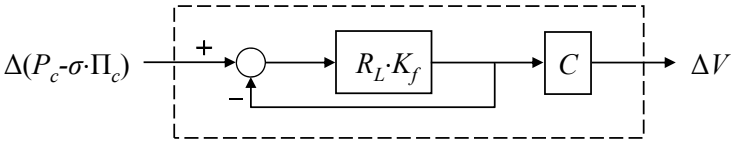

B

Variable	Edema
R_L	Impaired outflow edema
K_f	Enhanced inflow edema

	K_f high	K_f low	
R_L high	$EG \approx C$	$EG \approx C$	Compliance-Dominated gain
R_L low	$EG = \frac{C \cdot R_L \cdot K_f}{1 + R_L \cdot K_f}$	$EG = \frac{C \cdot R_L \cdot K_f}{1 + R_L \cdot K_f}$	Multivariate C, R_L, K_f gain

Figure A-6: A) Graphical representation of the Edemagenic Gain concept. Edemagenic Gain (*EG*) forms a "transfer function" relating changes in effective microvascular driving pressure $\Delta(P_c\text{-}\sigma \cdot \Pi_c)$ to changes in interstitial fluid volume ΔV. B) Edemagenic Gain takes on a simpler form when parameters have large or small values. When the effective lymphatic resistance (R_L) is significantly elevated (as in the case of impaired outflow edema), only interstitial compliance (C) determines Edemagenic Gain. In other cases, including enhanced inflow edema (as in the case of increased microvascular filtration), all three parameters, interstitial compliance (C), effective lymphatic resistance (R_L), and microvascular filtration coefficient (K_f) determine Edemagenic Gain.

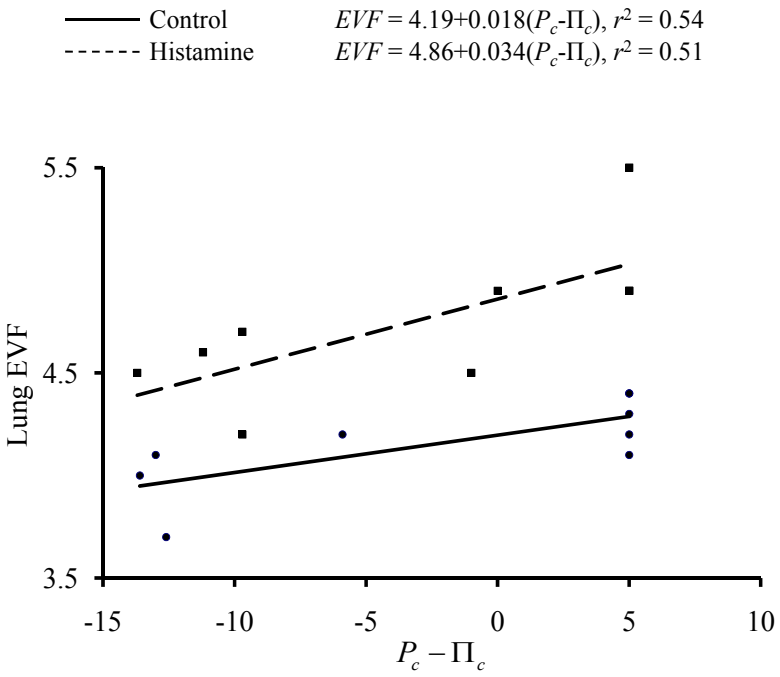

Figure A-7: Extravascular fluid volume (EVF) of sheep lung as a function of effective microvascular driving pressure (P_c-Π_c) for the control group (n = 11) and after infusion of histamine (n = 9). The regression line of the control and histamine data represented by solid and dashed lines, respectively. Edemagenic Gain for the histamine group is approximately double the control group (0.018 ml/g·mmHg vs. 0.034 ml/g·mmHg).

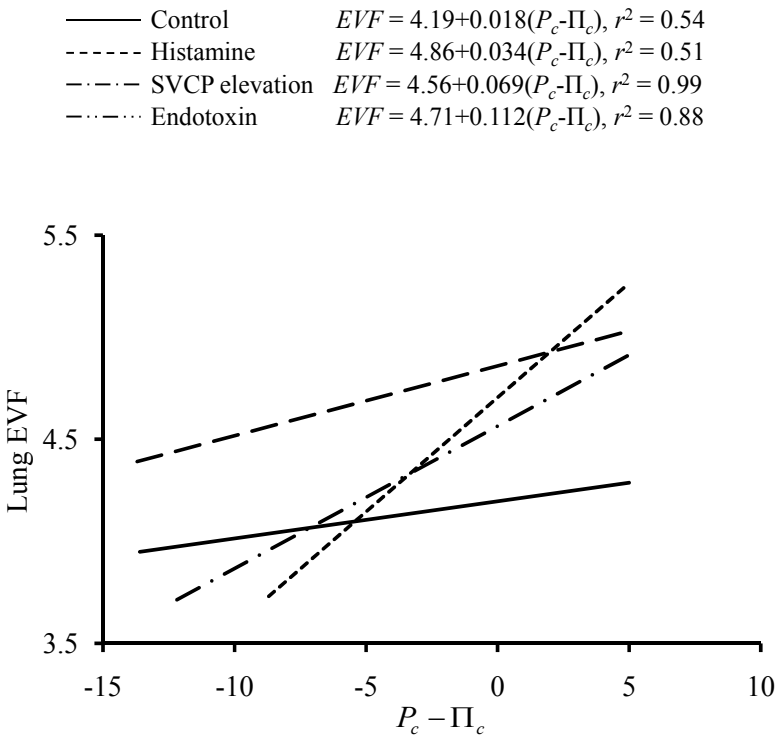

Figure A-8: Change in extravascular fluid volume (EVF) in response to change in effective microvascular driving pressure in controls, with histamine infusion, with endotoxin infusion, and superior vena caval pressure elevation (SVCP). Edemagenic Gains of the three intervention groups are larger than that of the control group (0.018 ml/g·mmHg). The endotoxin group (0.112 ml/g·mmHg) has larger Edemagenic Gain compared to the histamine group (0.134 ml/g·mmHg) and SVCP elevation group (0.069 ml/g·mmHg).

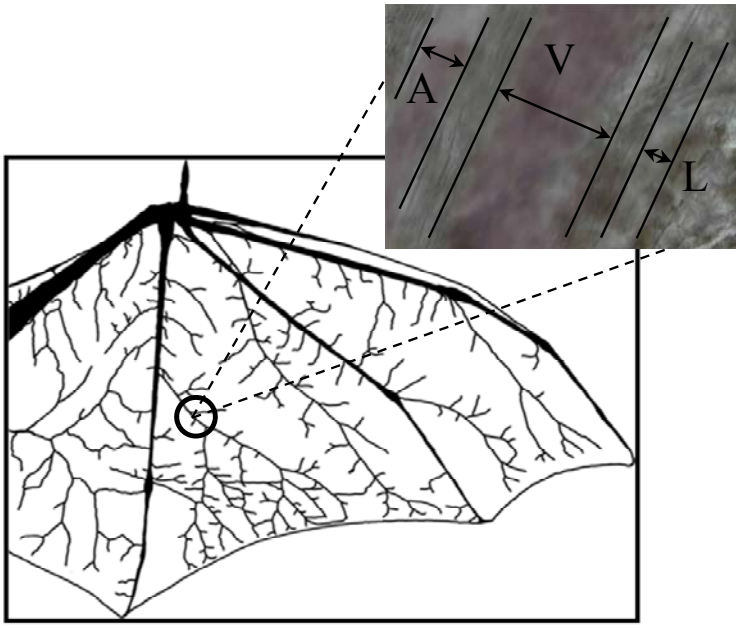

Figure A-9: Vessel network structure in the Pallid bat wing and location of the region of interest. A – arteriole, V – venule, L – lymphatic microvessel.

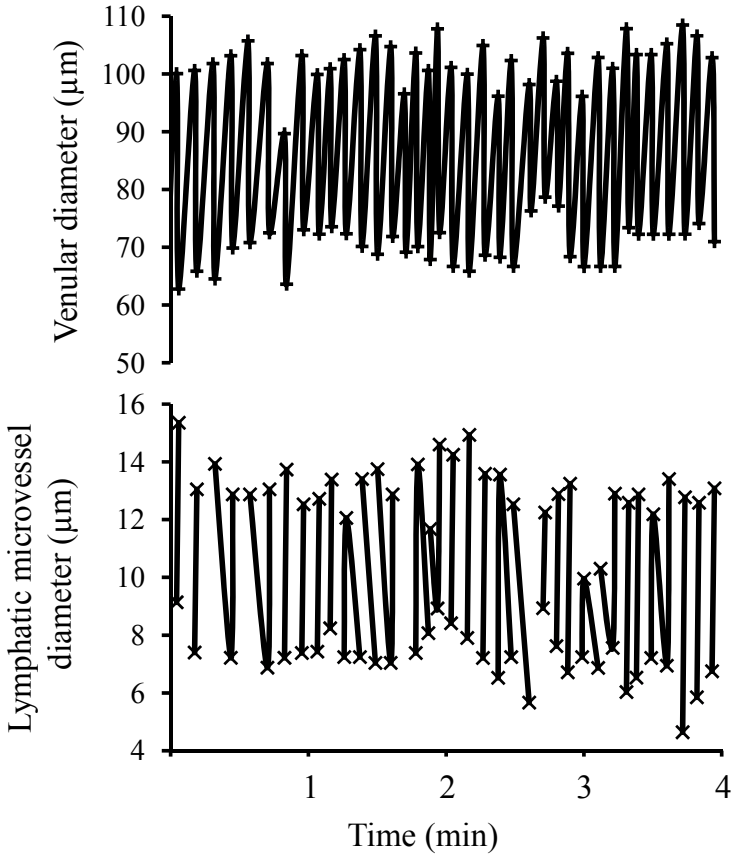

Figure A-10: Illustration of the oscillation of venular diameter (peak systolic and peak diastolic only) with time in a representative venule exhibiting venomotion and corresponding passive change in adjacent lymphatic microvascular diameter. Discontinuities in the illustrated lymphatic vessel diameter correspond to the active change in diameter due to intrinsic contraction.

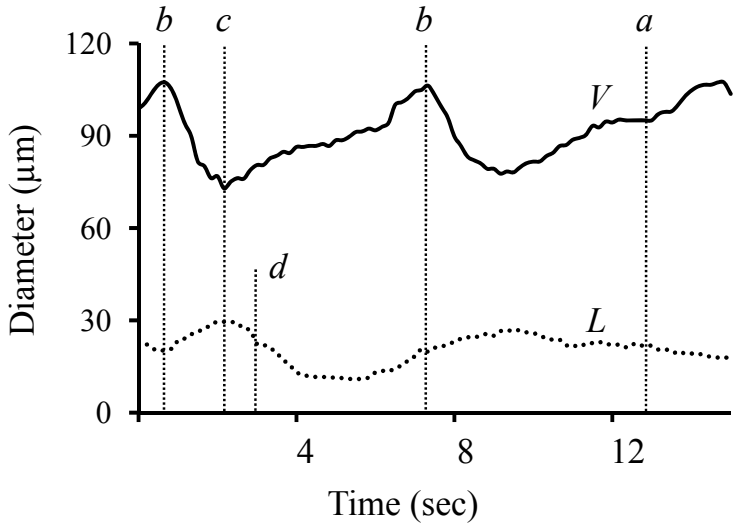

Figure A-11: Illustration of critical time points along the contraction cycles of a representative pair of adjacent venule (*V*) and lymphatic vessel (*L*). **a**: beginning venular dilation, **b**: time of peak venular diastole, **c**: time of peak venular systole, **d**: onset of active lymphatic contraction. The time **b** to **b** represents the venomotion period. The time **c** to **d** represents the time delay (Δt) between peak venular systole and onset of the active lymphatic contraction.

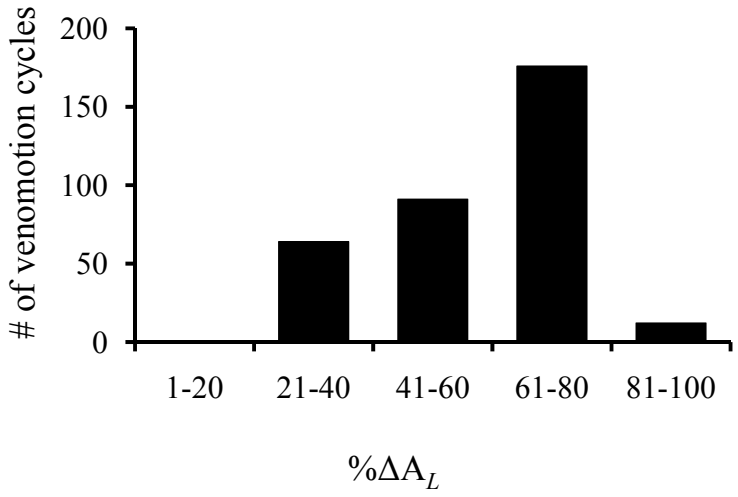

Figure A-12: Percent change in lymphatic microvascular cross-sectional area (%ΔA_L) due to passive expansion and compression by adjacent venule exhibiting venomotion.

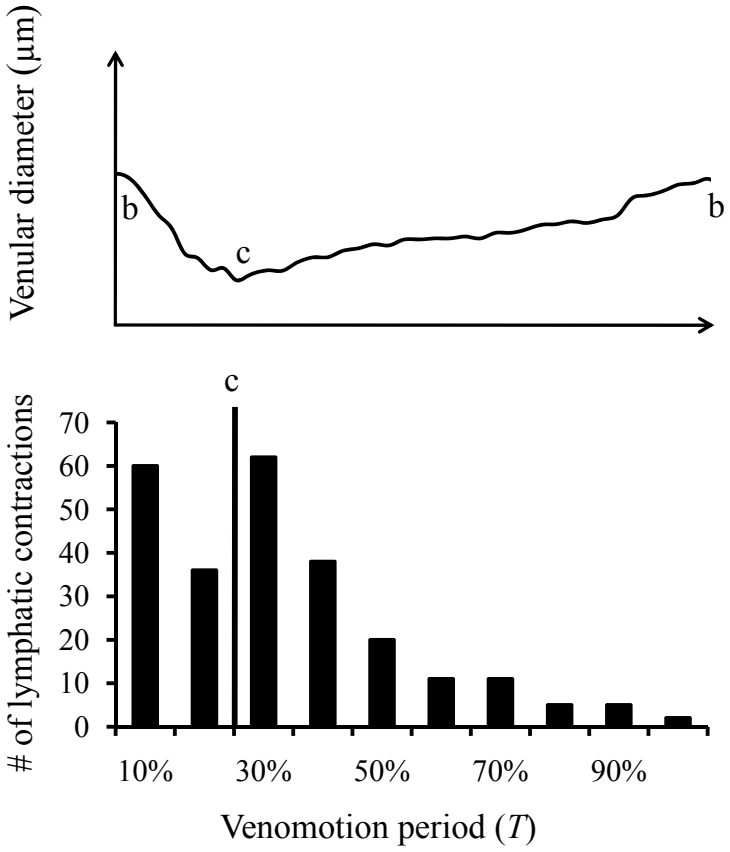

Figure A-13: Distribution of lymphatic microvascular contractions occurring after the onset of venous contraction expressed relative to the venomotion period (*T*). The bimodal distribution corresponds to venular dilation and contraction activity (within the first 20.99±6% of *T*). C corresponds to the time of peak venular systole that occurs within the venomotion period (b to b).

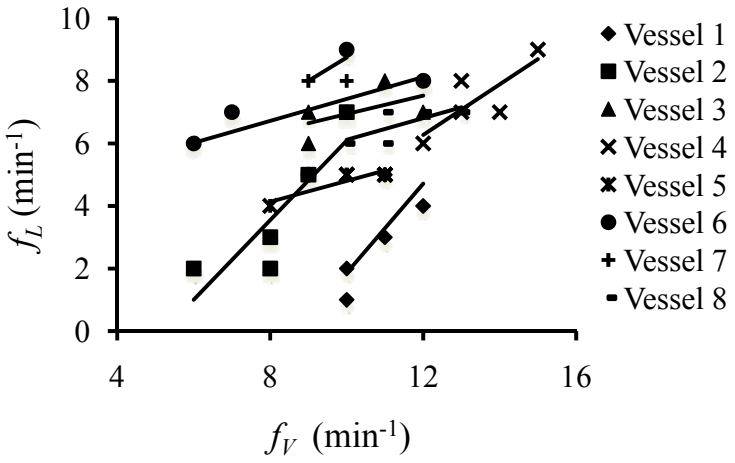

Figure A-14: Positive correlation between venomotion frequency (f_V) and lymphatic microvascular contraction frequency (f_L) with spontaneous venomotion (p<0.001, n=8). Linear regression analysis was performed using data from a five minute period.

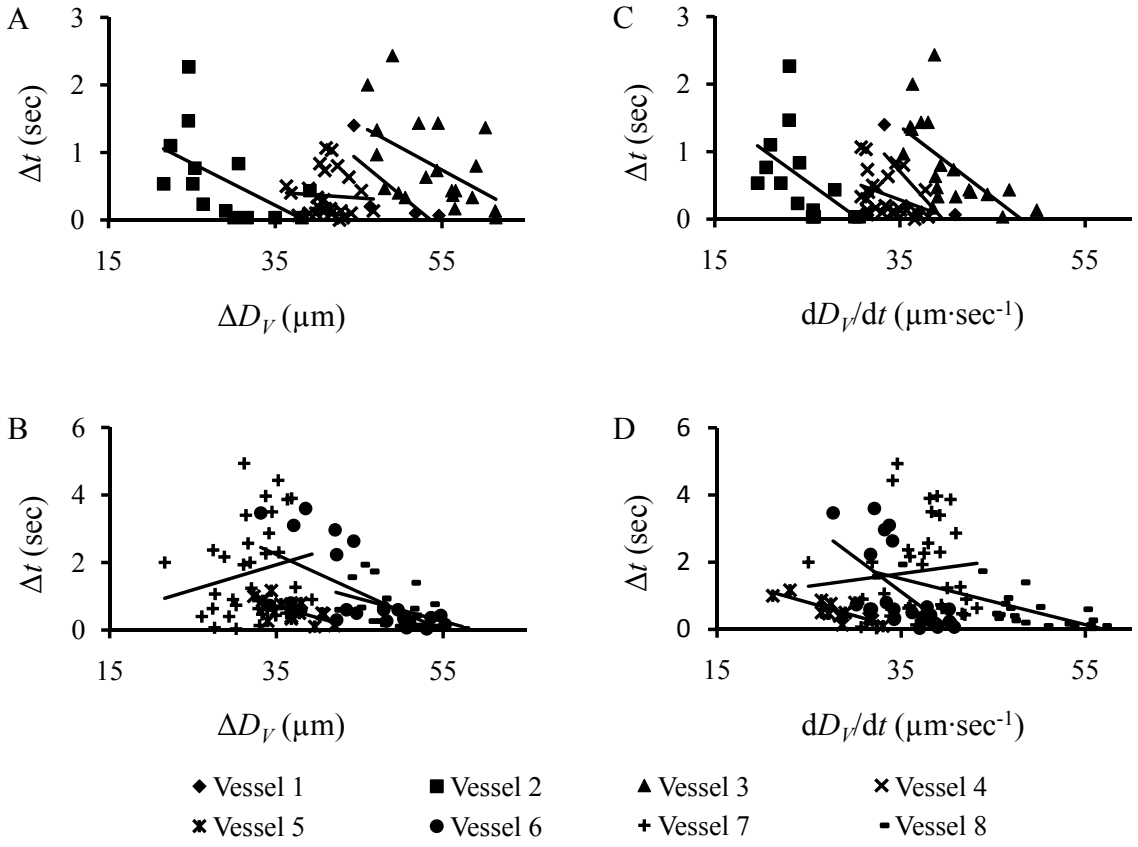

Figure A-15: The coordination between venomotion and lymphatic microvascular contractions depends on and the magnitude (ΔD_V) and velocity (dD_V/dt) of changes in venular diameter (n=8). Vessels 1-4 plotted separately from vessels 5-8 for clarity. A) Time delay vs. magnitude of changes in venous diameters for vessels 1-4. B) Time delay vs. magnitude of changes in venous diameters for vessels 4-8. As the magnitude of venomotion increases, the time delay (Δt) between peak venular systole and onset of lymphatic microvascular contraction is reduced ($p<0.001$). C) Time delay vs. velocity of vessel wall in vessels 1-4. D) Time delay vs. velocity of vessel wall in vessels 5-8. As the velocity of venomotion increases, the time delay between peak venular systole and onset of lymphatic microvascular contraction is reduced ($p<0.001$).

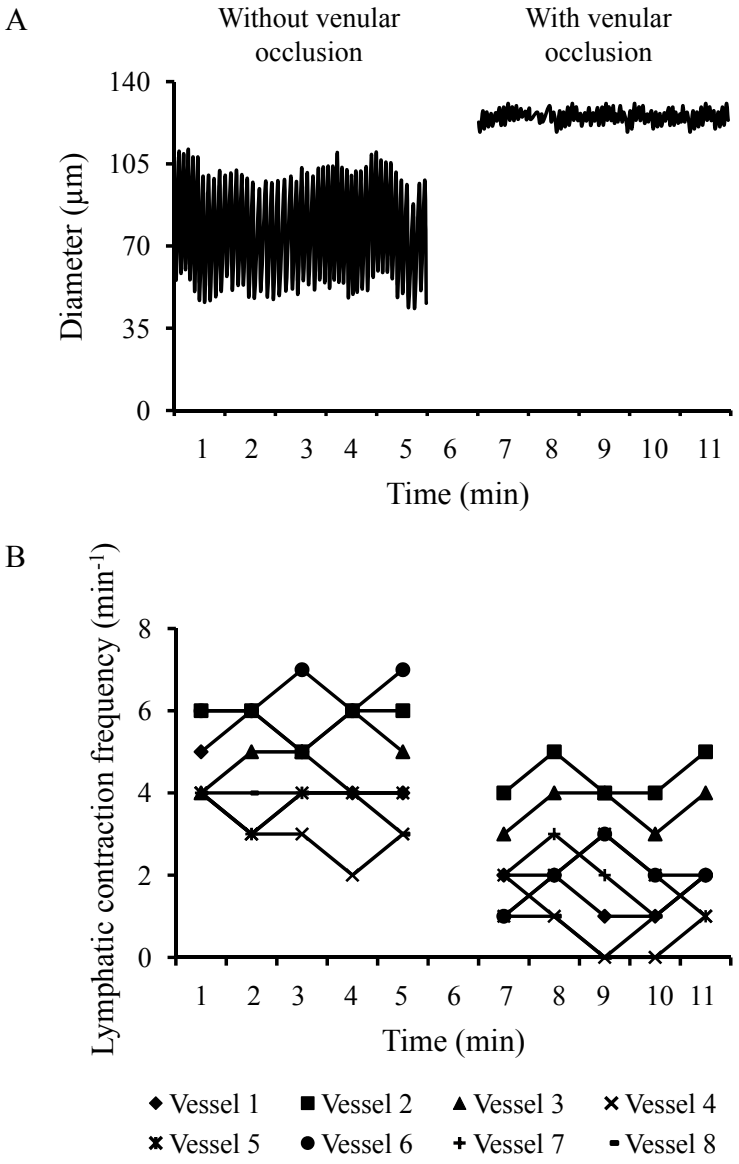

Figure A-16: Effect of venular occlusion on venomotion and contraction frequency of the adjacent lymphatic microvessel. A) Diameter tracing of a representative venule before and after complete venular occlusion shows venular dilation and abolished venomotion [as previously reported (30)] in response to increased venular transmural pressure. B) 54.3±20% decrease in lymphatic contraction frequency was observed with complete venular occlusion (n=8, $p<0.001$), indicating that venomotion mechanically triggers lymphangion contraction. Data could not be collected for approximately one minute while vessel was in the process of being occluded.

APPENDIX B

Table B-1. A) Comparison between the predicted values of interstitial fluid pressure (P_i) and interstitial protein concentration (C_i) calculated from *Eq. 3.8* and previously reported values. B) Effect of variation in K_f on estimated P_i and C_i. Increase in K_f results in increase in P_i and decrease in C_i. C) Effect of variation in σ on estimated P_i and C_i. Increase in σ results in decrease in P_i and C_i. [Values for P_p were assumed; $\alpha = 0.37$ (70, 71)]

A

Animal model	**Inter-vention**	**Values of other parameters**	**Estimated**		**Measured**	
			P_i	C_i	P_i	C_i
Dog lung	Control	R_L = 76 (37), K_f = 0.07 (43, 68), P_c = 7 (52), C_c = 58 (74), σ = 0.62 (122), PS = 0.07 (122), P_p = 20, P_{out} = 2	-2.2	31	-2.7 (97)	35 (74)
Dog skeletal muscle	Base line	R_L = 200 (91), K_f = 0.007 (8), P_c = 24 (50), C_c = 54 (160), σ = 0.72 (122), PS = 0.03 (122), P_p = 25, P_{out} = 2	-0.4	23.3	-0.1 (160)	22.4 (160)
Dog liver	Control	R_L = 74 (91), K_f = 0.3 (61), P_c = 7 (94), C_c = 60 (94), σ = 0.02 (122), PS = 1.6 (122), P_p = 20, P_{out} = 2	5.9	59.8	6 (94)	56.7 (94)
Dog small intestine	Control	R_L = 34 (91), K_f = 0.37 (79), P_c = 10 (79), C_c = 60 (94), σ = 0.7 (122), PS = 0.09 (60), P_p = 20, P_{out} = 2	-0.6	24.4	0 (80)	-
Sheep lung	Base line	R_L = 100 (93), K_f = 0.014 (45), P_c = 14.34 (45), C_c = 74 (45), σ = 0.48 (122), PS = 0.02 (122), P_p = 20, P_{out} = 2	-2.4	42.5	-	44.7 (45)

B

Animal model	**Inter-vention**	**Values of other parameters**	**K_f = 0.07**		**K_f = 0.11**	
			P_i	C_i	P_i	C_i
Dog lung	Control	R_L = 76 (37), P_c = 7 (52), C_c = 58 (74), σ = 0.62 (122), PS = 0.07 (122), P_p = 20, P_{out} = 2	-2.2	31	-1.3	30.7

Table B-1 continued.

C

Animal model	Inter-vention	Values of other parameters	σ = 0.48		σ = 0.89	
			P_i	C_i	P_i	C_i
Dog lung	Control	R_L = 76 (37), K_f = 0.07 (43, 68), P_c = 7 (52), C_c = 58 (74), PS = 0.07 (122), P_p = 20, P_{out} = 2	-0.2	36.6	-6.7	22.9

Table B-2: The range of parameter values affecting Edemagenic Gain, estimated from previously published reports. K_f : microvascular filtration coefficient; R_L : effective lymphatic resistance; C : interstitial compliance.

Ref. #	**Animal Model**	**Intervention**	**R_L ($cmH_2O \cdot min/\mu l$)**
(93)	Sheep lung	Control	0.54 ± 0.47
		Left atrial pressure elevation	0.24 ± 0.3
(39)	Canine lung	Extrapulmonary vessel	0.042 ± 0.03
		Intrapulmonary vessel	0.026 ± 0.02
Ref. #	**Animal Model**	**Intervention**	**K_f (ml/min·mmHg·100g)**
(68)	Canine lung	Left atrial pressure elevation	0.07
(98)	Canine lung	Left atrial pressure elevation	0.08
(41)	Canine lung	Pulmonary arterial and venous pressure elevation	0.11 ± 0.06
(43)	Canine lung	Pulmonary venous pressure elevation	0.07 ± 0.01
(149)	Rabbit lung	Pulmonary arterial pressure elevation	1.0
(52)	Canine lung	Pulmonary arterial and venous pressure elevation	0.07 ± 0.01
(35)	Canine lung	Pulmonary arterial and venous pressure elevation	0.21 ± 0.09
(58)	Canine lung	Transpulmonary pressure elevation	0.042 ± 0.02
			0.037 ± 0.011
Ref. #	**Animal Model**	**Intervention**	**C (ml/g·mmHg)**
(58)	Canine lung	Transpulmonary pressure elevation	0.137 ± 0.094
(102)	Rabbit lung	Control	0.019
		Pulmonary arterial and venous pressure elevation	0.025
(121)	Canine lung	Control	0.042
		Pulmonary arterial pressure elevation	0.565
(112)	Rabbit lung	Pulmonary arterial and venous pressure elevation	0.005
(114)	Canine lung	Transpulmonary pressure elevation	0.024

Table B-3: Sensitivity of Edemagenic Gain (EG) to various parameters. K_f : microvascular filtration coefficient; R_L : effective lymphatic resistance; C : interstitial compliance.

When $R_L \cdot K_f << 1$		
Parameter	**Change in parameter**	**Change in EG**
C	100%	100%
R_L	100%	$\approx 95\%$
K_f	100%	$\approx 95\%$

When $R_L \cdot K_f = 1$		
Parameter	**Change in parameter**	**Change in EG**
C	100%	100%
R_L	100%	$\approx 50\%$
K_f	100%	$\approx 50\%$

APPENDIX C

Nonlinear forms of the protein extravasation equation. Based on the principles of irreversible thermodynamics, Kedem and Katchalsky characterized solute transport across homoporous, sieving membranes (*Eq. C1*) (84). In this formulation, the convective and diffusive processes responsible for protein extravasation are considered independent of each other. On the other hand, the Patlak-Hoffman formulation (*Eq. C2*) (123) considers simultaneous convection and diffusion of proteins through the same pathway. In fact, their formulation generalizes the Hertzian formulation for sieving membranes, recognized as the gold standard for non-sieving membranes (18). The Manning formulation (*Eq. C3*) (103) is a linear approximation of Patlak-Hoffman formulation, assuming small J_V. The Taylor-Granger formulation (*Eq. 3.3*) (147) is the linear empirical approximation of Kedem-Katchalsky formulation. Except for the Kedem-Katchalsky formulation, the two-well accepted formulations (*Eqs. C2* and *C3*), along with Taylor-Granger formulation, suggest that C_L/C_c approaches (1-σ) with increasing J_V, i.e., lymph protein concentration (C_L) approaches a constant value at high J_V.

$$J_{sV}^{KK} = J_V(1-\sigma)\frac{(C_c - C_i)}{\ln\frac{C_c}{C_i}} + (C_c - C_i)PS \qquad (C1)$$

$$J_{sV}^{PH} = \frac{J_V(1-\sigma)(e^{\frac{J_V(1-\sigma)}{PS}}C_c - C_i)}{e^{\frac{J_V(1-\sigma)}{PS}} - 1} \qquad (C2)$$

$$J_{sV}{}^{M} = J_V(1-\sigma)\frac{C_c + C_i}{2} + (C_c - C_i)PS \qquad (C3)$$

Comparison of numerical solutions for protein extravasation. Various comparative studies have reported the accuracy of different microvascular protein extravasation characterizations. One such study by Breseler et al. (18) compared the Kedem-Katchlasky and Manning formulations to the Patlak-Hoffman formulation. The Taylor-Granger formulation (147) has not been included in such studies. In the present work, an approach similar to that of Breseler et al. was used to compare the accuracy of the J_{sV} estimation by the Taylor-Granger formulation (*Eq. 3.3*) with those of Kedem-Katchlasky (*Eq. C1*), Patlak-Hoffman (*Eq. C2*), and Manning (*Eq. C3*). As reported by Breseler et al. (18), the Patlak-Hoffman formulation is considered as the gold standard for comparison purposes. The ratio of errors in J_{sV} estimation is determined with *Eqs. C4a* and *C4b*. *Equation C4a* compares the Taylor-Granger formulation with the Kedem-Katchlasky formulation, and *Eq. C4b* compares the Taylor-Granger formulation with the Manning formulation.

$$R1 = \frac{\left|J_{sV}{}^{PH} - J_{sV}{}^{KK}\right|}{\left|J_{sV}{}^{PH} - J_{sV}{}^{TG}\right|} \qquad R1 > 1;\ \textit{Eq. 3.4 better approximates Eq. C1} \qquad (C4a)$$

$$R2 = \frac{\left|J_{sV}{}^{PH} - J_{sV}{}^{M}\right|}{\left|J_{sV}{}^{PH} - J_{sV}{}^{TG}\right|} \qquad R2 > 1;\ \textit{Eq. 3.4 better approximates Eq. C1} \qquad (C4b)$$

Figure A-5A illustrates $R1$ as a function of J_V with C_i/C_c = 0.1, 0.5 and 0.9 (σ = 0.6, PS = 0.118). Figure A-5B illustrates $R2$ as a function of J_V with C_i/C_c = 0.1, 0.5 and 0.9 (σ =

0.6, PS = 0.118). The Taylor-Granger formulation better approximates the Patlak-Hoffman formulation with increasing J_V than the others.

APPENDIX D

Derivation of Edemagenic Gain. In this formulation, interstitial hydrostatic pressure (P_i), microvascular fluid filtration (J_V), and lymphatic outflow (J_L) are considered to be functions of interstitial fluid volume. The microvascular reflection coefficient (σ) is considered to be constant, and the effect of changes in microvascular filtration on interstitial colloid osmotic pressure is neglected. A piecewise linear relationship between interstitial hydrostatic pressure and interstitial fluid volume is assumed (*Eq. 4.1*). Interstitial compliance, reciprocal of the slope of this relationship, determines the effect of change in interstitial fluid volume on interstitial hydrostatic pressure. Substituting this relationship (*Eq. 4.1*) into the Starling-Landis Equation (*Eq. 3.1*), indicates how transmicrovascular flow is affected by changes in interstitial fluid volume.

$$J_V = K_f \cdot \left[\left(P_c - P_o - \frac{V}{C} \right) - \sigma \cdot \left(\Pi_c - \Pi_i \right) \right] \qquad (D1)$$

By substituting *Eq. D1* and the Drake-Laine Model (*Eq. 3.4*) into *Eq. 4.2*, the effect of changes in interstitial fluid volume on lymphatic flow can be reformulated into an integral,

$$V = \int \left(K_f \cdot \left[\left(P_c - P_o - \frac{V}{C} \right) - \sigma \cdot \left(\Pi_c - \Pi_i \right) \right] - \frac{\left(P_o + \frac{V}{C} - P_{out} \right)}{R_L} \right) \cdot dt + V_{initial} \qquad (D2)$$

where $V_{initial}$ is the initial volume.

Integrating *Eq. D2* results in interstitial fluid volume as an analytical equation that includes a function of time (t).

$$V = \frac{C \cdot R_L \cdot K_f}{1 + R_L \cdot K_f} \cdot \left[\left(P_c - P_o \right) - \sigma \cdot \left(\Pi_c - \Pi_i \right) \right] - \frac{C}{1 + R_L \cdot K_f} \cdot (P_o - P_{out}) - \frac{C \cdot R_L}{1 + R_L \cdot K_f} \cdot \exp\left[-\left(\frac{1 + R_L \cdot K_f}{C \cdot R_L} \right) \cdot t \right] + V_{initial} \quad (D3)$$

Assuming all parameters are constant, the difference between two volumes is obtained as a result of changes in effective microvascular driving pressure (P_c-$\sigma \cdot \Pi_c$) and expressed as "Edemagenic Gain" (*Eq. 4.3*)

In previous attempts to characterize the change in interstitial fluid volume in response to change in the effective microvascular driving pressure (53), interstitial hydrostatic pressure was considered constant. The negative feedback provided by changes in interstitial hydrostatic pressure, therefore, was neglected. The change in interstitial fluid volume given by the time integral of the inflow and outflow rate (*Eq. 4.2*) would thus be

$$V = \left[K_f \cdot \left((P_c - P_i) - \sigma \cdot (\Pi_c - \Pi_i) \right) - J_L \right] \cdot t + V_{initial} \quad (D4)$$

The relation between change in interstitial fluid volume and change in effective microvascular driving pressure is obtained from *Eq. D4*.

$$\frac{\Delta V}{\Delta \left(P_c - \sigma \cdot \Pi_c \right)} = K_f \cdot t \quad (D5)$$

The formulation of Edemagenic Gain presented in the current work (*Eq. 4.3*) is preferred over *Eq. D5*, because *Eq. 4.3* does not require the assumption that interstitial hydrostatic pressure is constant, and thus it requires fewer assumptions.

The formulation of Edemagenic Gain represented by *Eq. 4.3* can be modified to characterize the relationship of ΔV to changes in the microvascular driving pressure determined by P_c, Π_c, Π_i, and σ. The modified Edemagenic Gain thus becomes a function of the microvascular reflection coefficient, σ as well as interstitial colloid osmotic pressure Π_i.

$$EG = \frac{\Delta V}{\Delta(P_c - \sigma \cdot (\Pi_c - \Pi_i))} = \frac{C \cdot R_L \cdot K_f}{1 + R_L \cdot K_f} \qquad (D6)$$

VITA

Name: Ranjeet Manohar Dongaonkar

Address: Department of Physiology & Pharmacology, Texas A&M University, College Station, TX 77843-4466

Email Address: ranjeet@tamu.edu

Education: B.E., Production Engineering, Dr. Babasaheb Ambedkar Marathwada University, 1998

M.S., Mechanical Engineering, Texas A&M University, 2003

Ph.D., Biomedical Sciences, Texas A&M University, 2008